Graduate School ETD Form 9
(Revised 12/07)

PURDUE UNIVERSITY
GRADUATE SCHOOL
Thesis/Dissertation Acceptance

This is to certify that the thesis/dissertation prepared

By N. Luke Thomas

Entitled A NEW APPROACH FOR HUMAN IDENTIFICATION USING THE EYE

For the degree of Master of Science in Electrical and Computer Engineering

Is approved by the final examining committee:

Yingzi Du
Chair

Maher Rizkalla

Brian King

To the best of my knowledge and as understood by the student in the *Research Integrity and Copyright Disclaimer (Graduate School Form 20)*, this thesis/dissertation adheres to the provisions of Purdue University's "Policy on Integrity in Research" and the use of copyrighted material.

Approved by Major Professor(s): Yingzi Du

Approved by: Yaobin Chen 1/28/2010
Head of the Graduate Program Date

Graduate School Form 20
(Revised 1/10)

PURDUE UNIVERSITY
GRADUATE SCHOOL

Research Integrity and Copyright Disclaimer

Title of Thesis/Dissertation:
A NEW APPROACH FOR HUMAN IDENTIFICATION USING THE EYE

For the degree of Master of Science in Electrical and Computer Engineering

I certify that in the preparation of this thesis, I have observed the provisions of *Purdue University Teaching, Research, and Outreach Policy on Research Misconduct (VIII.3.1)*, October 1, 2008.*

Further, I certify that this work is free of plagiarism and all materials appearing in this thesis/dissertation have been properly quoted and attributed.

I certify that all copyrighted material incorporated into this thesis/dissertation is in compliance with the United States' copyright law and that I have received written permission from the copyright owners for my use of their work, which is beyond the scope of the law. I agree to indemnify and save harmless Purdue University from any and all claims that may be asserted or that may arise from any copyright violation.

N. Luke Thomas
Printed Name and Signature of Candidate

1/28/2010
Date (month/day/year)

*Located at http://www.purdue.edu/policies/pages/teach_res_outreach/viii_3_1.html

A NEW APPROACH FOR HUMAN IDENTIFICATION USING THE EYE

A Thesis
Submitted to the Faculty
of
Purdue University
by
N. Luke Thomas

In Partial Fulfillment of the
Requirements for the Degree
of
Master of Science in Electrical and Computer Engineering

May 2010
Purdue University
Indianapolis, Indiana

ACKNOWLEDGMENTS

First and foremost, I would like to gratefully acknowledge my thesis advisor, Dr. Yingzi (Eliza) Du, for her guidance, supervision, and knowledge during my course of study, research, and thesis work. I would like to express my gratitude to my thesis committee members, Dr. Maher Rizkalla and Dr. Brian King, for their time and helpful comments. I thank Ms. Valerie Lim Diemer, Ms. Jane Simpson, and Ms. Sherrie Tucker for their constructive suggestions and help formatting this thesis.

I also would like to sincerely thank my lab mates Mr. Craig Belcher, Mr. Zhi Zhou, Mr. Tron Artavatkun, and Mr. Kai Yang for the technical discussions, their help and support in collecting data for this thesis research, and friendship. I would like to express my appreciation to those subjects who contributed their biometric information for use in the IUPUI multi-wavelength database.

I would also like to acknowledge the Department of Computer Science at the University of Beira Interior for providing the UBIRIS database. This work was partially funded by the ONR Young Investigator Award #: N00014-07-1-0788. I would like to thank the ONR for their generous financial support.

Finally, and most importantly, I would like to thank my wife for her support, dedication, and love. She has graciously accepted the difficulties and problems that have accompanied my graduate studies. Without her support and inspiration, this work would not have happened.

TABLE OF CONTENTS

Page

Page

LIST OF TABLES

LIST OF FIGURES

Figure Page

ABSTRACT

Thomas, N. Luke. M.S.E.C.E., Purdue University, May 2010. A New Approach For Human Identification Using The Eye. Major Professor: Yingzi Du.

The vein structure in the sclera, the white and opaque outer protective covering of the eye, is anecdotally stable over time and unique to each person. As a result, it is well suited for use as a biometric for human identification. A few researchers have performed sclera vein pattern recognition and have reported promising, but low accuracy, initial results. Sclera recognition poses several challenges: the vein structure moves and deforms with the movement of the eye and its surrounding tissues; images of sclera patterns are often defocused and/or saturated; and, most importantly, the vein structure in the sclera is multi-layered and has complex non-linear deformation. The previous approaches in sclera recognition have treated the sclera patterns as a one-layered vein structure, and, as a result, their sclera recognition accuracy is not high. In this thesis, we propose a new method for sclera recognition with the following contributions: First, we developed a color-based sclera region estimation scheme for sclera segmentation. Second, we designed a Gabor wavelet based sclera pattern enhancement method, and an adaptive thresholding method to emphasize and binarize the sclera vein patterns. Third, we proposed a line descriptor based feature extraction, registration, and matching method that is scale-, orientation-, and deformation-invariant, and can mitigate the multi-layered deformation effects and tolerate segmentation error. It is empirically verified using the UBIRIS and IUPUI multi-wavelength databases that the proposed method can perform accurate sclera recognition. In addition, the recognition results are compared to iris recognition algorithms, with very comparable results.

1. INTRODUCTION AND LITERATURE REVIEW

1.1 Biometrics

To prevent further terrorist attacks, our government must be able to properly secure its borders, strategic assets (both military and civilian), and sensitive information while still honoring the rights of its population. This is a difficult and complicated task — how can one verify a person's identity with certainty while still honoring their civil and personal rights? How can one do this knowing that there are individuals specifically attempting to mislead or defraud the system?

Biometrics is the identification of humans using intrinsic physiological, biological, or behavioral characteristics, traits, or habits. Biometrics have the potential to provide this desired ability — to unambiguously and discretely identify a person's identity — more accurately and conveniently than other options.

Examples of biometric modalities include face, iris, hand, fingerprint, gait, typing, speech, and others. In general, biometrics can be divided into two broad categories –

- Physiological biometrics — those that identify an individual from an intrinsic physiological or biological trait (ex. face, iris, fingerprint, etc)
- Behavioral biometrics — those that identify an individual from a behavioral trait (ex. gait, typing, etc)

In general, physiological biometrics are more stable.

In the past decade, advances in computing power have made automated biometric systems realistic alternatives or supplements to traditional security systems. For users, biometric systems can reduce or eliminate the need to retain a key or remember a

password, can speed up user throughput, and can be less intrusive. For example, at a border or security checkpoint, a biometric system could provide a high-confidence identification of a user while they walk through a checkpoint rather than requiring them to stop, produce some identification, and be interviewed by security personnel. From a system standpoint, biometric systems can check much larger databases than are realistic with traditional security systems, are more consistent, do not have racial or personal biases, and can be cheaper to operate.

1.2 Iris Recognition

Iris recognition is identification of humans using the iris — the annular, colored portion of the eye. Cooperative iris recognition systems have been practically implemented for border control, access control, and other systems. Recently, there has been much interest in expanding the operation of iris recognition into non-cooperative situations.

1.2.1 Cooperative Iris Recognition

Cooperative iris recognition is currently the most accurate biometric modality, with large scale implementations currently being used for human identification for border control in the United Arab Emirates [1], for the United States Army [2], in airports around the world [3], and elsewhere. Cooperative iris recognition systems are characterized by the cooperative nature of the human participants — they are both cognizant and compliant in the recognition process. Most existing commercially available iris recognition systems use algorithms originally developed by John Daugman [4-7]. These systems require frontal gaze, well-focused, well-centered, high quality images of the eye acquired in the near-infrared (NIR) wavelengths.

In [1], Daugman reports on the results of over 200 billion cross comparisons of irises in the United Arab Emirates border control database. In this paper, he reports that

the lowest observed matching score for eye images that were from different subjects was in the range of .26, which corresponds to a theoretical false match rate of 1 in 200 billion. By changing the decision threshold from .26 to .22, he also reports a theoretical false match rate of 1 in $5x10^{15}$, which would enable all-to-all matching of a population of approximately 70.7 million (slightly more than the total population of the United Kingdom) with just a single false accept. While these results are exceptional, and have certainly enabled very accurate positive human identification within constrained operational settings with large databases, they are still not adequate for positive human identification for the entire population of the United States of America (~304 million as of 2008) with similar arbitrarily small false acceptance rates.

Cooperative iris recognition systems are produced by Iridian, LG, and other companies. Many of these systems require the user to actively position themselves in the systems operational area, and follow some instructions given by the system. An example commercial system that has low habituation requirements is the Iris-On-The-Move system by the Sarnoff Corporation [8]. This system uses a bank of high definition video cameras to acquire video images of users as they walk thru a portal, and extract and match the users from their irises. However, this system still requires both frontal gaze eye orientation and near-infrared (NIR) illumination, and is still considered compliant for these reasons.

Figure 1.1 shows four example images from an example cooperative iris recognition database — the ICE database [9]. Notice that all the images have high signal-to-noise ratio; frontal gaze eye orientation; and very little noise, specularities, or occlusion.

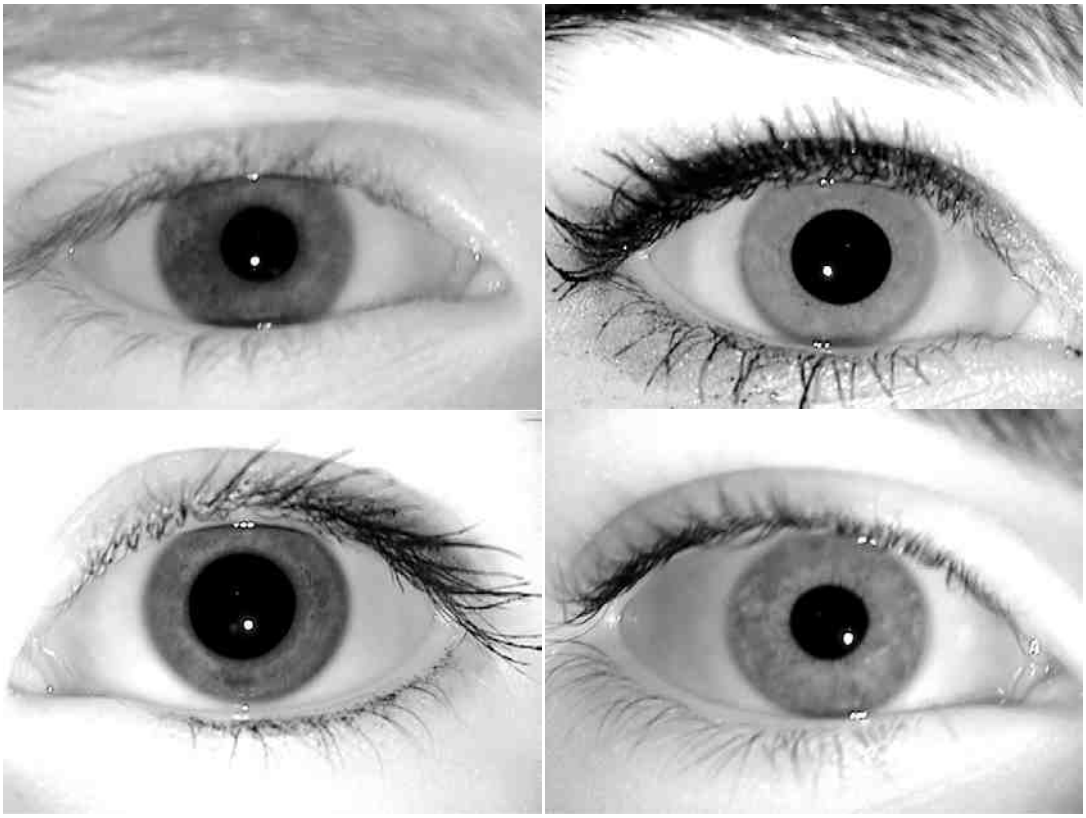

Figure 1.1 Example cooperative iris images

1.2.2 Non-Cooperative Iris Recognition

Non-cooperative iris recognition is characterized by the lack of active participation by the individuals being identified. Non-cooperative systems would be more convenient for users, more flexible in their deployment, and could be used with video surveillance applications. Some examples of different operating environments that would be considered non-cooperative include surveillance, no-habituation systems, and long acquisition distance identification systems. In each of these situations, the users may not be aware of the identification system, are not required to actively participate with the system, and may have little or no previous experience interacting with the system.

The IUPUI Biometrics and Pattern Recognition Lab has developed experimental non-compliant iris recognition systems; however, few, if any, commercially available non-compliant iris recognition methods exist. Example, currently theoretical, non-compliant systems would allow for surveillance of a volume of space, for example a border control check point, and would identify each user as they entered the space, regardless of their intent to be recognized, their knowledge of the systems existence, or specific actions within the systems recognition region. These types of systems do not currently exist in practice, but are the 'ideal' goal for the progression of existing systems.

In the Biometrics and Pattern Recognition Lab at IUPUI, we have designed and developed non-cooperative iris recognition systems and components including non-compliant iris segmentation [10, 11], iris image quality measures [12, 13], and non-cooperative iris recognition methodologies [14, 15]. Figure 1.6 shows some example non-cooperative images from the IUPUI multi-wavelength database. Note, in particular, that the images have more noise, less consistent focus, more iris occlusion, and inconsistent frontal gaze eye orientation, as compared to the cooperative iris recognition images.

1.2.3 Visible Wavelength Iris Recognition

Some researchers have worked on implementation of iris recognition with visible wavelength images. This would allow for more broad application of iris recognition to non-compliant situations, since it is very technically complicated to provide the necessary level of NIR illumination for a non-compliant situation. However, because dark colored iris patterns are not as apparent under visible light as compared to NIR illumination, the matching results for visible light iris matching systems have typically been significantly worse than comparable results with near-infrared images. Figure 1.3 shows some example images from the UBIRIS database [16], an iris recognition database that was acquired in the visible wavelengths using color images.

1.2.4 Multiple Wavelength Iris Recognition

Recently, some researchers have focused on multiple wavelength or multi-spectral iris recognition [17, 18]. These types of systems look to use some of the differential information between the multiple acquisition wavelengths to provide more discriminating identification results, as opposed to typical systems which use a single acquisition wavelength (either NIR, visible, or otherwise). Currently, the initial results for multiple wavelength iris recognition show some promise, however, the most accurate results still incorporate the typical NIR illumination used in compliant iris recognition systems.

1.2.5 Limitations of Iris Recognition

For all the success that iris recognition has had, there are some limitations for iris recognition using existing algorithms. First, for NIR acquired images, it is difficult to properly illuminate the subject at a distance of over 20 meters. Most NIR iris systems acquire iris images at a distance of less than one foot, and even systems such as the Iris-On-The-Move system require an illuminator very close to the subject to provide proper NIR illumination. This is impractical for a surveillance system where the camera-to-subject distance would be much greater than one foot, and the acquisition volume could be very large. Second, accurate segmentation of the iris boundaries in grayscale near-infrared illuminated images requires a very high signal-to-noise ratio, and much of the discriminating color information that could be used for segmentation is lost. This makes the accurate segmentation of the iris region more difficult than it could be were the images acquired in color. Third, darkly colored irises perform much worse than lightly colored irises when identified using existing algorithms in the visible spectrum. This is due to the high absorption of visible light by dark colored irises, so that little of the identifying structure of the iris can be imaged and extracted.

1.3 Retina Recognition

Retina recognition [19, 20] is another eye-based biometric, but it uses the structure of the retina, the lining of the inner surface of the eye, to identify people. Because the retina is an internal structure of the eye, it is not practical to acquire non-compliant images of the retina in humans. From a practical standpoint, acquisition of retinal images is typically considered intrusive enough that even for many compliant recognition systems it is not practical or ideal.

Additionally, the vein structure of the retina is not deformed with the movement of the eye, and as such retinal vein recognition algorithms are not applicable for sclera vein recognition applications [21, 22].

1.4 Sclera Recognition

Sclera recognition is identification of a human using the sclera, the 'white of the eye.' It offers several benefits over other eye-based biometrics that make it well-suited for non-compliant recognition situations.

1.4.1 The Sclera and Conjunctival Vasculature

The sclera is the white and opaque outer protective covering of the eye. The sclera completely surrounds the eye, and is made up of four layers of tissue — the episclera, stroma, lamina fusca, and endothelium [23]. The conjunctiva is a clear mucous membrane, made up of epithelial tissue, and consists of cells and underlying basement membrane that covers the sclera and lines the inside of the eyelids[1]. In general, the conjunctival vascular is hard to see with the naked eye at a distance. Figure 1.2 shows an image of an eye under visible wavelength illumination with identification of the sclera vein patterns. For young children, the blood vessels in sclera area could be blue, but for adults, the blood vessels are red in color. The structure of the blood vessels in the sclera

[1] http://en.wikipedia.org/wiki/Conjuctiva

are well suited to be used as a biometric — they are an internal organ that is visible without undue difficulty and they are anecdotally stable over time and unique for each person [23, 24]. Therefore, the vein patterns in the sclera could be used for positive human identification.

In previous works, identification of users using the sclera region has been referred to as ‘conjuctival vasculature recognition.’ However, as the conjunctiva is the top-most transparent layer of the sclera and images of the sclera region capture more than just this top-most layer, it is more accurate to refer to the system as performing ‘sclera recognition.’

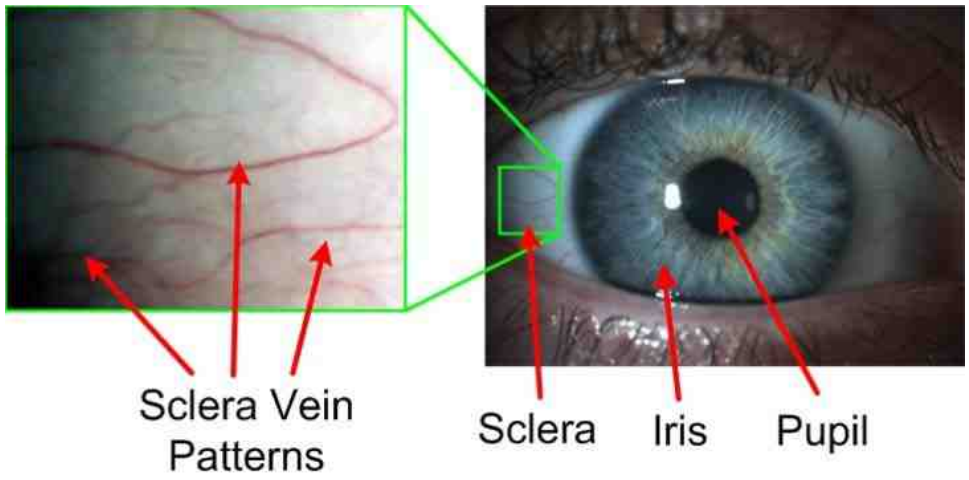

Figure 1.2 The structures of the eye and sclera region

1.4.2 Advantages of Sclera Recognition

In comparison to iris recognition, sclera recognition offers several benefits, especially for non-compliant or non-cooperative situations. First, sclera recognition does not require imaging the eye in the near-infrared wavelengths. This allows for less constrained imaging requirements, including imaging at very long stand-off distances, may not require additional illumination, and, perhaps, enable the use of existing imaging systems to acquire and match individuals (such as using existing surveillance systems to

acquire the images). Second, sclera recognition does not require frontal gaze images of the eye. For sclera recognition, assuming that the entire sclera region was enrolled for matching, off-angle eyes reveal more of the sclera vein pattern for matching. Thus, even an individual who was actively attempting to avoid detection or recognition by looking away from the matching system would be unable to avoid presenting a valid biometric pattern for identification.

1.4.3 Previous Works on Recognition in the Sclera Region

The eye region has been extensively used for positive human identification by using, most notably, the iris and, less so, the retina. However, little work has been done that uses the sclera region for identification.

In [25], Derakhshani *et. al.* first proposed using 'conjunctival vascular' patterns for user identification. The conjuctiva is the thin top layer of the sclera region, and the conjuctival vasculature is the system of veins and arteries in this layer. They used contrast limited adaptive histogram equalization (CLAHE) to enhance the green color plane of the RGB image, and a multi-scale region-growing approach to identify the sclera veins from the image background. For matching, they proposed a multi-level matching approach — a coarse approach to sub divide the database, and a fine approach to specifically match a user from the preliminary sub-divided segment of the database, as found from the course approach. For the course approach, they utilize Hu's 7-th skew-invariant moments [26] to perform preliminary matching. For the fine approach, as described in the paper, they propose 2 methods — a minutiae based approach and a two-dimensional correlation approach. In this work, they used a small database of 24 images composed of 2 images of the left and right eyes of 6 users. With manual segmentation, they reported 100% matching accuracy for both matching approaches.

Later, in [27], Derakhshani and Ross used a texture-based neural network classifier, manual segmentation of the sclera region, and adaptive thresholding and

enhancement on the vasculature images. For matching, they used a single hidden layer feed forward neural network with 512 input nodes, 300 hidden nodes, and 50 output nodes. In this work, the authors collected a database of 50 users, with images acquired in 2 sittings, with a 20 minute lapse in between, at acquisition distances of 1, 5, and 9 feet, for 300 total images. They trained their neural network classifier with the first sitting's data (150 images), and tested with the second sitting. Their reported results are presented in Table 1.1.

Table 1.1 Reported EER's for Derakshani and Ross [27]

	Reported EER:		
	1 Foot (50 images)	3 Feet (50 images)	9 Feet (50 images)
One Eye	6.50%	7.40%	11.00%
Both Eyes	4.30%	8.80%	9.20%

Most recently, in [28] Crihalmeanu *et. al.* used an semi-automated k-means clustering algorithm to estimate the sclera region from the RGB values of the pixels in the color sclera images, and used manual intervention to correct for misclassified boundaries (in particular, the lower eyelid boundary). They proposed a registration method that incorporates local affine and global smoothing transformations that locally deforms the template image to provide the best registration with the target image. Using the 'cross-correlation between non-specularity regions' in the registered images, they report an equal error rate around 25%, using their internally acquired database of 50 users. In particular, note that this most recent work is the first, and only, that does not use manual segmentation to ensure that the sclera regions to be matched are already well segmented and registered.

It is important to note that the previous three works have different lead authors, but they are all from the same academic group — Ross, Derakhshani, and Crihalmeanu. These initial works have shown that the sclera can be used for accurate human

identification. As they pointed out in the conclusion of [28], for practical use of the sclera vasculature as a biometric identifier there is more work that is necessary.

1.4.4 Sclera Recognition Databases

Due to the relative 'newness' of sclera vein recognition, there are not currently any publicly available databases specifically for sclera vein pattern recognition. Additionally, since sclera vein patterns are not readily visible under near-infrared illumination, the normal illumination for iris recognition algorithms, only iris image databases that are acquired under visible light illumination are potentially useful for sclera vein recognition applications. In this research, 2 databases are used – the UBIRIS database and the IUPUI multi-wavelength database.

1.4.4.1 UBIRIS Database

The UBIRIS database [16] is a publicly available database with iris images acquired in color. The database consists of 1877 images acquired from 241 users acquired in two sessions. The images are predominately frontal gaze. The database is available with multiple image resolutions, with the maximum image resolution being 800 by 600 pixels. In session 1, noise was minimized and the images were attempted to be acquired in focus. However, in session 2, noise effects were not minimized, ambient light was not normalized, and a significant number of the images have very poor focus. In both sessions, the images are generally cropped such that the eye is predominately centered and the eye region well-cropped in the images. Some example images from the UBIRIS database, session 1, are presented in Figure 1.3.

Figure 1.3 Example images from the UBIRIS database, session 1. The top row shows good quality images, the middle row shows images of mid- to poor- quality, and the bottom row shows poor quality images.

In the session 1 database, the primary difference between good and poor quality images is image focus and/or eyelid occlusion. For some images, the iris and sclera region are very poorly focused, which reduces the visual clarity of the image and in many cases makes the sclera vein patterns difficult, or impossible, to reliably identify by either automatic or manual methods. Examples of this type of poor image quality can be seen in the bottom left and middle images in Figure 1.3. For the case of significant eyelid occlusion, such as the bottom right image in Figure 1.3, even if the image is well-focused, if there is not enough sclera region visible in the image, one cannot extract enough sclera vein pattern to reliably identify the individual.

For the session 2 database, the images are of very poor quality for sclera recognition. Figure 1.4 shows some example images from the session 2 database. Note that the overall image quality is much worse, and much less consistent than in the session 1 database. In particular, the focus on the sclera region is very inconsistent, which makes the session 2 database very poor for sclera recognition. Figure 1.5 shows some example images from the same user across the two databases. The top row is an example image from the user in the session 1 database, and the bottom row is an example image from the same user in the session 2 database. Note that in the session 2 images, the image quality is much worse, and in particular the focus in the sclera region is very poor in the session 2 images.

Figure 1.4 Example images from the UBIRIS database, session 2. The top row shows good quality images, the middle row shows images of mid- to poor- quality, and the bottom row shows poor quality images.

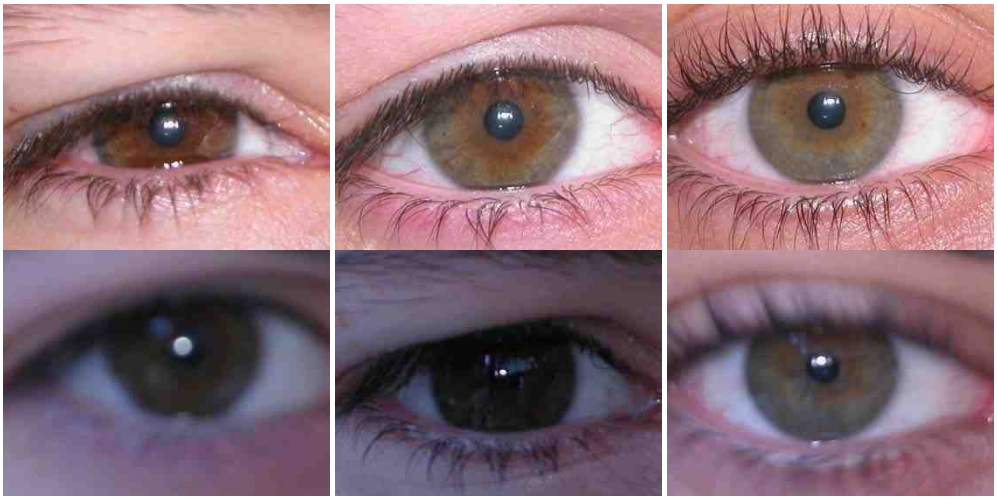

Figure 1.5 Example images from the same user in the UBIRIS database. Top row – session 1, bottom row – session 2

1.4.4.2 IUPUI Multi-wavelength Eye Database

The IUPUI multi-wavelength database is an internally acquired database of video images of user's eye and the surrounding regions with different eye gaze-angles, illumination wavelengths, and ambient illumination levels. The database is composed of 45 users, with two videos acquired of each user with at least 1 week of time between acquisitions. For each session, 32 videos were acquired – 8 different illumination wavelengths (420, 470, 525, 590, 610, 630, 660, and 820 nm), with and without ambient illumination, and both the user's left and right eyes. For each video, the user was asked to direct their gaze to 6 different gaze locations (centered, up, left, left-up, right, and right-up) during the video. Each image was acquired at a resolution of 1280 by 1024 pixels, with the eye generally centered in the image. In general, the eye regions are around 1000 pixels in width, about 200 pixels more than the UBIRIS database's maximum eye width. Users were asked to limit the movement of their head, but no restraints were used to otherwise limit their movement.

Figure 1.6 shows example images from the IUPUI multi-wavelength database for one user at a wavelength of 525nm with different gaze angles. Because the images were

acquired and focused manually, there is some difference in the detailed level of focus between the two sessions for each user and between the left and right sclera regions.

Figure 1.6 Example images from the IUPUI multi-wavelength database – 6 images from the same user and illumination wavelength (525 nm) with different gaze angles

Figure 1.7 shows 8 images of the same user and gaze angle, but with different illumination wavelengths. In particular, note that the sclera vein patterns presentation is different with different illumination wavelengths. In general, the sclera vein patterns are most apparent under wavelength 3 (525 nm), the third image from the upper left of the figure, which was the reason it was chosen for this work.

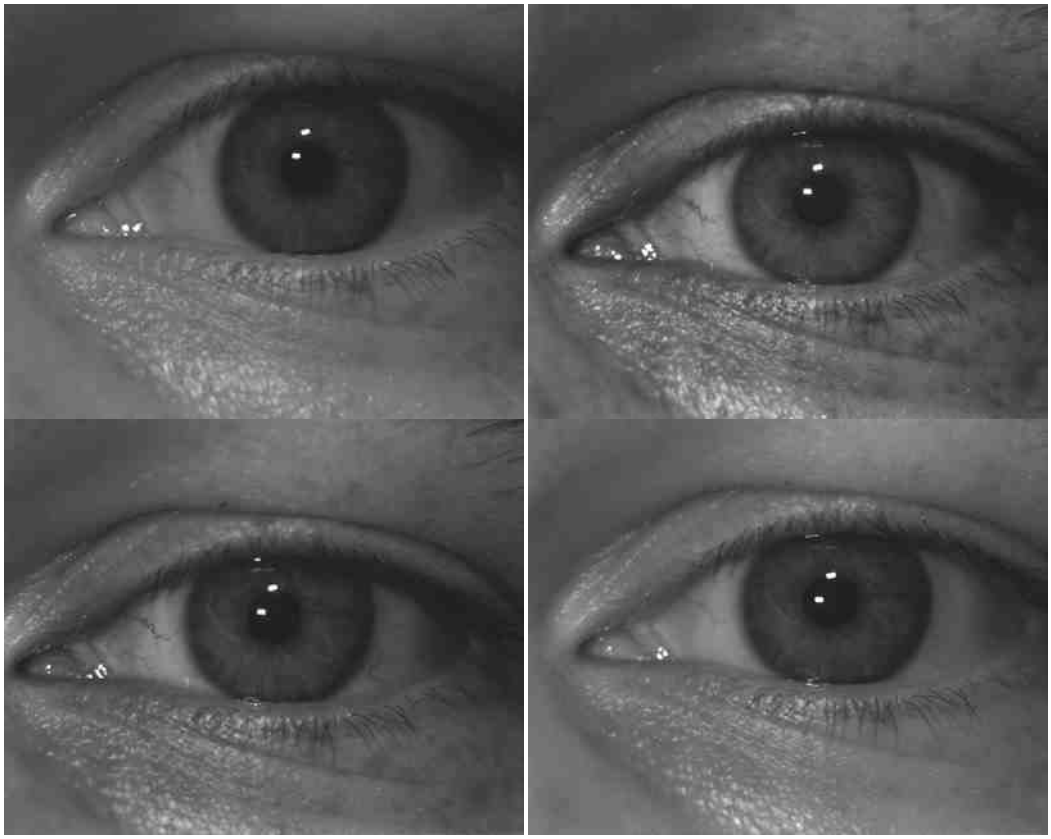

Figure 1.7 Example images from the IUPUI multi-wavelength database - 8 images of the same user and gaze angle acquired with different illumination wavelengths (from upper left: 420, 470, 525, 590, 610, 630, 660, and 820 nm)

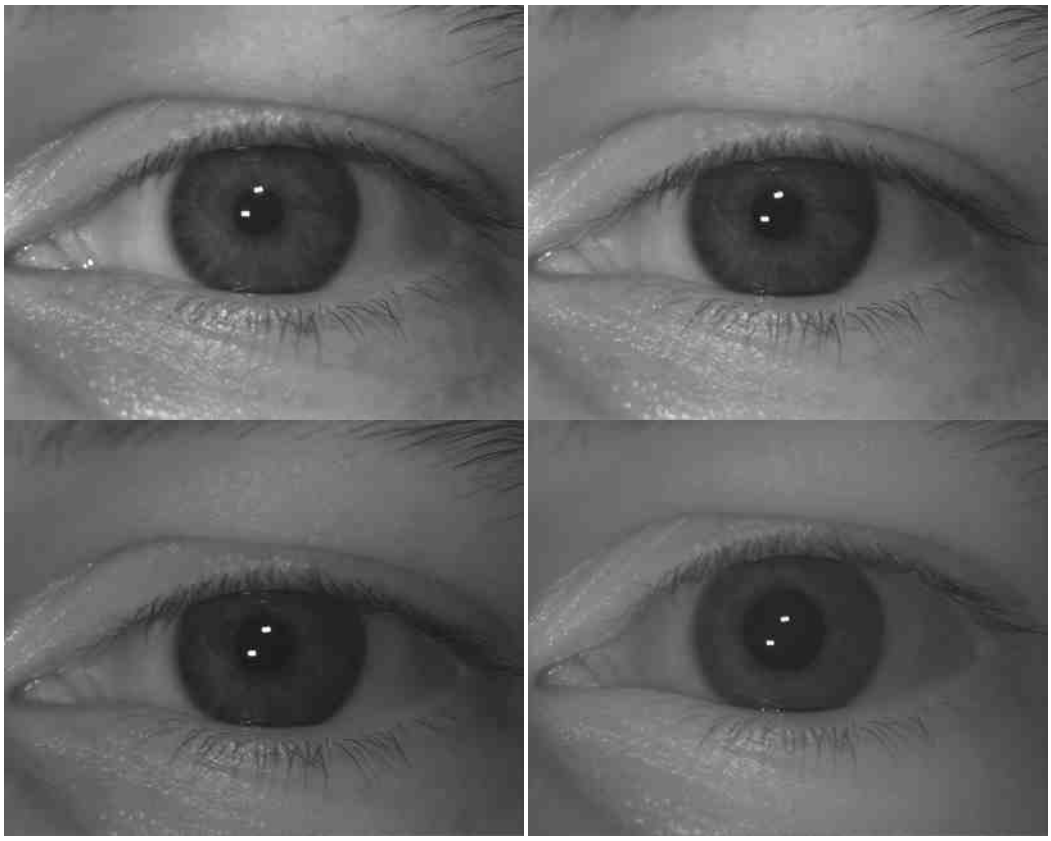

Figure 1.7 Continued

1.4.5 Sclera Recognition Challenges

Sclera recognition has several technical difficulties that make it difficult to implement in practice, including:

- The eye is a moving structure, and the sclera vascular patterns move and are deformed with this movement (including the movement of the eye and eyelids, and dilation/contraction of pupil).
- The sclera is reflective, so the sclera patterns may be out-of-focus or saturated.
- Most importantly, the vascular patterns in the sclera are composed of multiple layers, and as a result, there is complicated non-linear deformation of the patterns as the eye and/or the surrounding tissues move (such as the eyelids), Figure 1.8 and Figure 1.9.

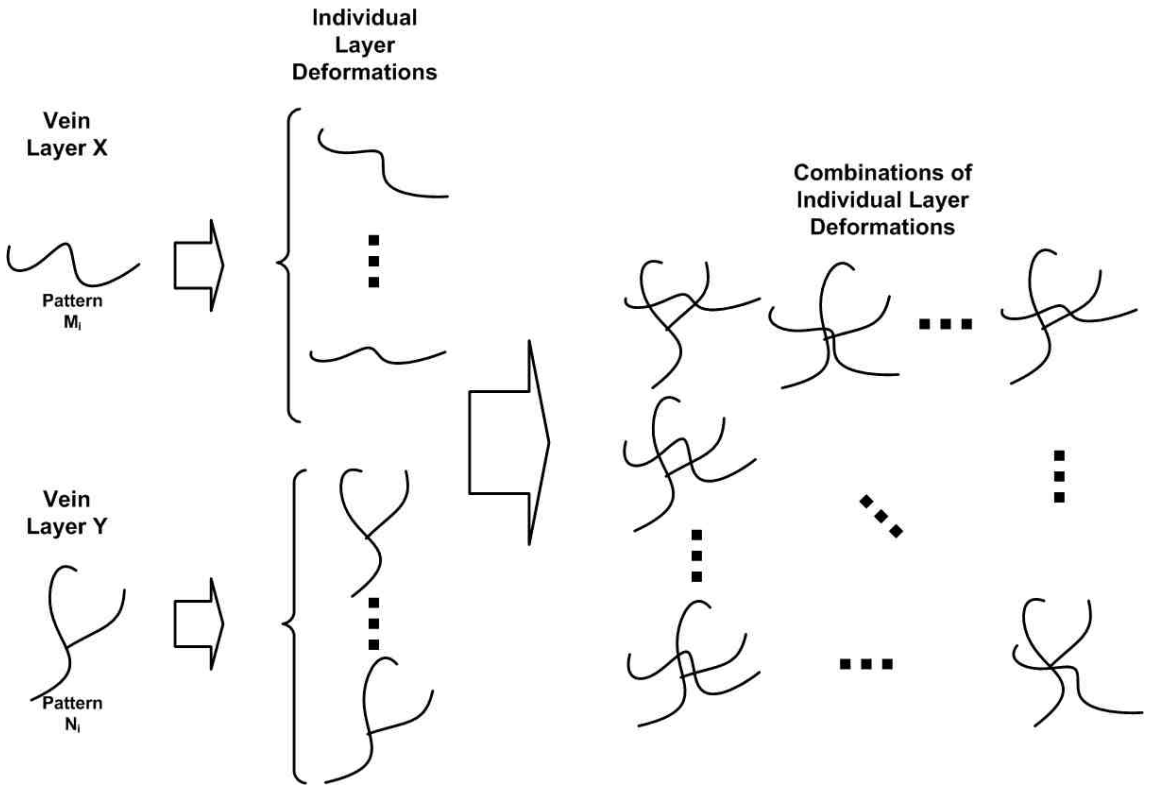

Figure 1.8 An example illustration of how different patterns can emerge from multiple independent layers

Figure 1.8 shows an example of some of the multitude of patterns that can emerge from the interaction of two independently deforming layers. On the left of Figure 1.8, we show two representative vein patterns, M and N, from vein layers X and Y, and then some of the myriad of individual layer deformations that these patterns can exhibit. The combination of the two patterns, M and N, due to the individual layer deformations can result in many different observable multi-layered non-linear deformations. Note, in particular, that the overall structure of the emergent pattern (crossing points, relation between vein landmarks, etc.) can change significantly with the multiple layers' interactions. Figure 1.9 shows an example of multi-layered deformation of sclera patterns from images of a real person. Figure 1.9(a) and Figure 1.9(b) were acquired in a sequence of video imagery of an eye within one second. The upper eyelid of the Figure 1.9(b) is a slightly more open, as compared to Figure 1.9(a). In the zoomed-in view of the sclera patterns, we see that that the vascular pattern is made up of multiple layers that

are moving relatively independently. Specifically, one can see that the 'curvy' vein, Y (with points A_1, B_1, and C_1) and the 'smooth' veins, X_1 (with points B_2 and C_2) and X_2 (with point A_2) have different relative positions in the two images. The 'smooth' veins, X_1 and X_2, stay relatively similar in position but their orientation shifts toward the lower right portion of the image, while the 'curvy' vein, Y, shifts down in Figure 1.9(b) but retains its orientation. Also, the vein structure (where the veins cross and their relation to each other) around points A_1 and A_2 is significantly different between the two images, and that the points B_1 and B_2 are separate in the top image, but are touching in the bottom. Again, this is due to the transition of the 'curvy' vein, Y, with respect to the straight vein, X_1.

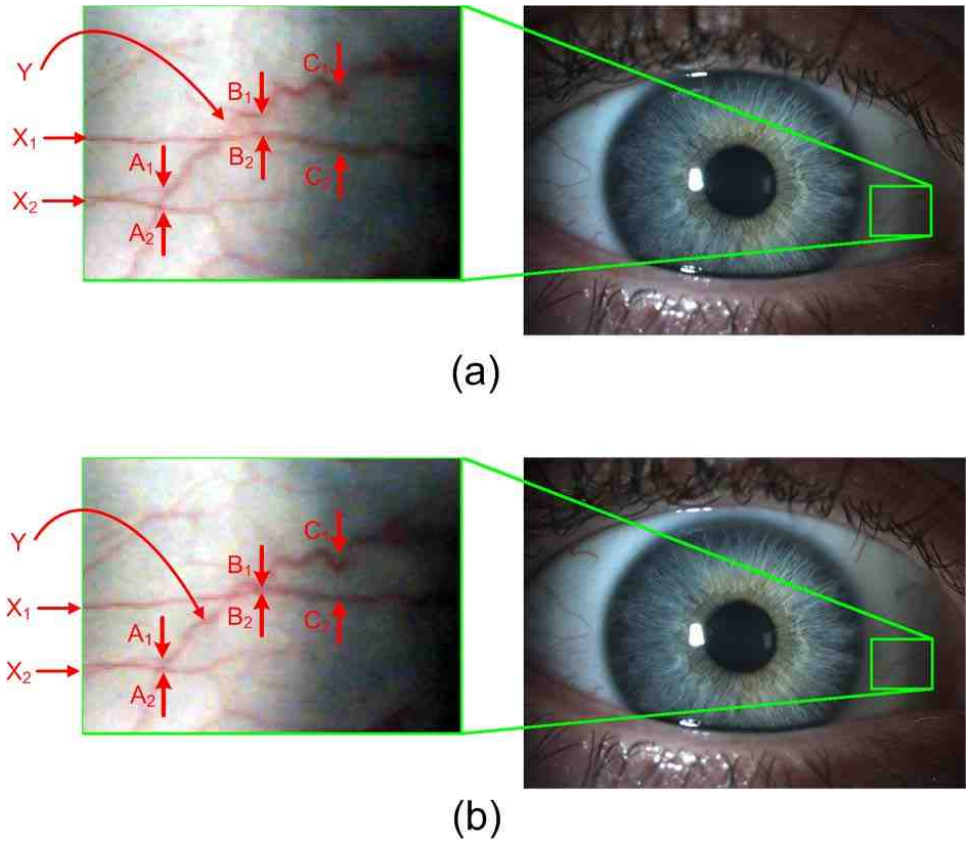

Figure 1.9 An example of layered non-linear deformations in multiple images of the same eye. In particular, note the areas as denoted by the arrows. Both images were acquired in a video sequence within one second.

2. OVERVIEW OF PROPOSED SYSTEM

2.1 Background of Vein Recognition

Vein recognition has been used and studied for personal identification, such as finger vein recognition, palm vein recognition, retina vein recognition, and sublingual vein recognition. Usually, the veins are described and matched with the assumption that the vein pattern is not multi-dimensional, and that the vein patterns will only have global translation or scaling [19, 29-35].

2.2 Vein Recognition vs. Sclera Recognition

Because the other previous vein recognition methods assume that the vein patterns are not multi-dimensional, these methods are not applicable for sclera vein recognition situations. Specifically, multiple independent layers will pose difficulties producing reliable matching results when the typical emergent qualities of the pattern (crossing point, relation between close veins, etc) are used for matching. As shown in Figure 1.8 and Figure 1.9, multiple independent layers can create many possible overall patterns, and as such the matching system should take this into account.

Previous vein recognition systems do not account for this type of change in the pattern, and as such they would not be consistently accurate for sclera recognition. Therefore, a new type of system needs to be developed that can account for these types of issues to allow for accurate results using sclera recognition.

2.3 Proposed Method

Figure 2.1 shows a simple block diagram of the proposed system, which is composed of 4 major components: sclera segmentation, feature extraction and enhancement, feature matching, and the matching decision.

For the sclera segmentation system, a system is developed that can accurately segment the sclera region using color images and does not require training. The proposed system estimates the sclera using the color information in the image, detects the iris and eyelid boundaries, and refines them using an active contour method. The goal of this system is to identify and extract the relevant portions of the sclera from the original image of the eye region for further processing and identification. The primary difficulties in this section are proper segmentation of the eyelid boundaries, especially the lower eyelid boundary near the tear duct, and segmentation of images with very little visible sclera region.

The feature extraction and enhancement system uses a bank of Gabor filters to extract the vein pattern from the segmented sclera region. The enhanced vein patterns are thresholded using an adaptive threshold, and thinned to a pixel wide skeleton using morphological operations. Finally, a novel line-descriptor method is used to describe and store the extracted vein pattern for recognition. The goal of this section is to reliably extract and describe the vein pattern in the sclera for use in identifying the user. The primary difficulties in this section are reliably extracting the vein structure and extracting the vein structure for low quality images.

The feature matching system uses a RANSAC-based registration system to register the sclera vein templates to achieve translation-, rotation-, and scaling-invariance. Then, a pair-wise distance measure is used to match the templates using their line descriptor sets. Finally, the matching score is determined from the weighted matching scores, and is used to determine if the two descriptors are a match. The goal of this section is development of a system that can consistently identify users from their

extracted vein pattern descriptors in the presence of noise, unusual vein presentations, and deformations. The primary difficulties in this section are addressing the complex non-linear deformation of the sclera vein patterns and developing an appropriate registration algorithm that does not over-fit and introduce false-matches into the matching results of the system.

Each of the preceding systems is described at length in the subsequent sections.

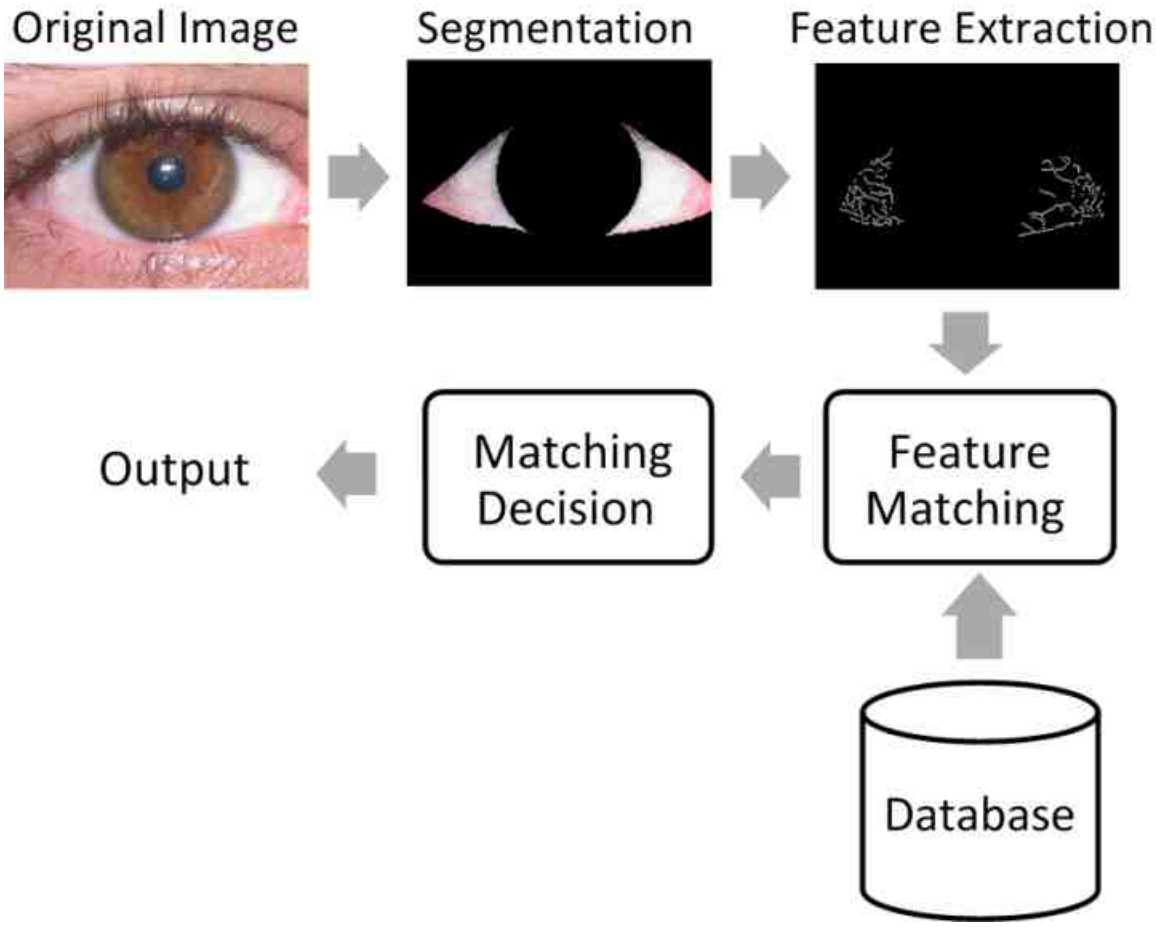

Figure 2.1 The proposed system

3. SCLERA SEGMENTATION

3.1 Review of Iris Image Segmentation Methods

Many researchers have worked on segmentation of the pupil and iris boundaries for compliant iris recognition [4, 6-8, 11-14, 36-52] for eye images in the near infrared (NIR) wavelengths. Historical examples include Daugman's integro-differential operator which searches for the optimum set of parameters, r, x_0, y_0, that describe a circle that maximizes the following equation.

$$\max_{r,x_0,y_0} \left| G_\sigma(r) * \frac{\partial}{\partial r} \oint_{r,x_0,y_0} \frac{I(x,y)}{2\pi r} ds \right| \tag{3.1}$$

Some researchers have used the circular Hough transform to search an edge detected image for the optimal circular representation of the iris or pupil [37, 46]. The circular Hough transform uses the accumulation of values in a parameter space to 'vote' for the most likely set of parameters for an object (such as a line or circle) in the image. Many other, more current, methods have been proposed and tested — active contours or 'snakes,' multi-scale approaches, geodesic active contours, etc. However, all of these methods used for compliant iris recognition require high-quality, frontal-gaze images to ensure that the iris and pupil boundaries are circular (or nearly circular) and the eye region boundaries are well defined, which may not be valid for sclera recognition applications.

In [53-55], Proenca *et al.* proposed segmentation algorithms for iris images in the visible wavelengths with the UBIRIS database. Especially relevant for this work is that he segments the sclera as an interim step in segmenting the iris, and uses visible wavelength images [54]. Training is necessary in this approach, as it uses a neural network for preliminary region classification.

In [54], Proenca segments the sclera as a preliminary step in segmentation of the iris boundaries for non-compliant color iris images. To segment the sclera, he uses a neural network classifier using a 20 element feature vector for each pixel in the image. The feature vector was composed of $\{x, y, H_{0,3,7}^{\mu,\sigma}(x,y), Cr_{0,3,7}^{\mu,\sigma}(x,y), Cb_{0,3,7}^{\mu,\sigma}(x,y)\}$. Where (x, y) is the pixels position, $H(\cdot)$ is the hue colorplane of the image, $Cr(\cdot)$ is the red chrominance colorplane of the image, and $Cb(\cdot)$ is the blue chrominance colorplane of the image. The subscripts indicate the features used (mean and standard deviation) and the radii used (0, 3, and 7 pixels).

For the classification, the neural network was a multi-layered perceptron feed-forward neural network with a single hidden layer. They used 20 input neurons, 30 hidden neurons, and 1 output neuron. For training they used the back-propagation algorithm, and trained with 50,000 randomly selected pixels from 30 training images equally distributed between 'sclera' and 'non-sclera.' Because they were using the sclera segmentation as a preliminary step for further segmentation of the iris boundary, they do not report the accuracy of the sclera segmentation.

In [11], Du and Arslanturk proposed a non-cooperative segmentation algorithm for video iris images. This system used a PCA-based clustering algorithm to quickly identify the iris pupil center, and a SVD-based conic fitting algorithm to fit a least-squares conic section to the detected iris and pupil boundary points for non-compliant video images.

3.2 Review of Previous Sclera Segmentation Methods

Segmentation of the sclera region is the first step in processing sclera images for sclera recognition. An ideal segmentation algorithm would properly identify only the sclera areas that contain useful information for identification, and remove all other areas. In particular, proper segmentation is very important for any biometric system — it provides the baseline for the systems accuracy. The "best" biometric identification

system cannot provide good accuracy if it is using poorly segmented results. As such, accurate segmentation of the desired region is of utmost importance to the overall system's results.

As stated earlier, sclera recognition is a relatively new biometric modality, in comparison to iris recognition, and as such, there are very few people who have worked on segmentation of the sclera region. Additionally, in comparison to iris segmentation, the sclera boundaries exhibit more intra-class variation and retain all of the difficulties that are faced in iris recognition — eyelid occlusion, specular reflections, low signal-to-noise ratio, etc. One advantage of sclera segmentation, when using color images, is that the additional information contained in the color information can be used to mitigate some of these issues and difficulties.

In [25], Derakhshani *et al.* first proposed the use of the sclera vasculature for biometric identification, they performed all segmentation manually. Additionally, in [27], they use manual segmentation of the sclera region to specify the region of interests. In this work, they claimed that they used a simple intensity-based routine that further segments the sclera region into smaller region of interests, but do not further define this process.

In [28], Crihalmeanu *et al.* presented a semi-automated system for sclera segmentation. They used a k-means clustering algorithm to cluster the color eye images into three clusters. Then, the three clusters were classified as sclera, iris, and background by classifying the cluster with the largest Euclidean distance to the RGB origin vector $[0, \quad 0, \quad 0]^T$. Similarly, the iris was classified as the cluster with the smallest Euclidean distance to the origin, and the background was the remaining cluster. Then, using these clustered regions, the convex hull of the iris region was removed from the convex hull of the sclera region to create a mask of the sclera region, and then manual intervention was performed to correct, if necessary, for incorrectly segmented portions of the image.

Table 3.1 shows the reported percentage of different image classes that required manual intervention, with a total of 35% of all images requiring manual intervention.

Table 3.1 Reported percentage of images requiring manual correction

Gaze		% Requiring manual Intervention	
	Acquisition Distance	Left Eyes	Right Eyes
Looking Left	near	45.52%	31.34%
	medium	36.57%	26.87%
	far	32.09%	29.10%
Looking Right	near	40.30%	41.79%
	medium	39.55%	38.06%
	far	26.12%	32.84%

In particular, they noted the lower boundary between the sclera and eyelids/eyelashes as a problematic area to accurately segment. This area, in particular near the tear ducts, is difficult to segment because the sclera in this region tends to be very vascular, so the color of the sclera and the color of the eyelid can be very similar. Additionally, the vasculature in this area can introduce a level of ‘texture’ in the sclera that can make segmenting the eyelid boundary using edge or gradient-based techniques difficult.

3.3 Proposed Sclera Segmentation Method

In this work, we proposed a new segmentation method for color images by first estimating the sclera region using the best representation between two color-based techniques, and then refining the boundary using the Fourier active contour method [7]. The block diagram of the segmentation algorithm is shown in Figure 3.1, which includes image downsampling, conversion to the HSV colorspace, estimation of the sclera region, iris and eyelid detection, eyelid and iris boundaries refinement, mask creation, and mask upsampling.

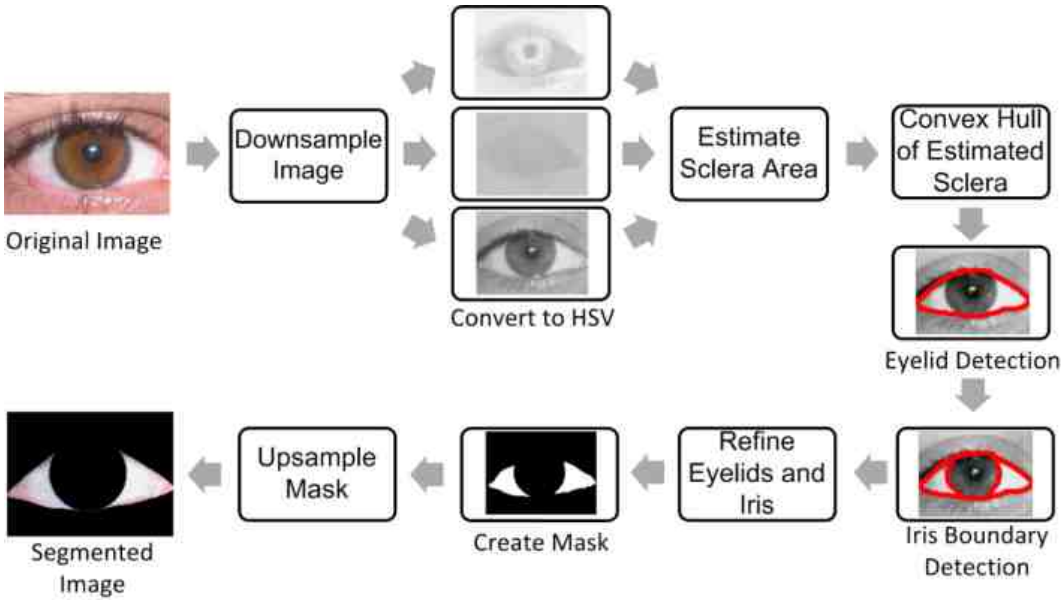

Figure 3.1 The proposed segmentation system

3.3.1 Downsampling the Image

To improve the segmentation efficiency, the input image is first downsampled to increase processing speed. For the UBIRIS image database, we downsampled the images by a factor of 5, which reduces the image size to 1/25th of its original size.

3.3.2 Conversion to HSV colorspace

The image is converted from the RGB colorspace to YCrCb colorspace and then to the HSV colorspace, to facilitate the use of simple segmentation heuristics in the HSV colorspace:

$$\begin{bmatrix} Y \\ C_R \\ C_B \end{bmatrix} = \begin{bmatrix} .299 & .587 & .114 \\ -.169 & -.331 & .499 \\ .499 & -.418 & -.0813 \end{bmatrix} \begin{bmatrix} R \\ G \\ B \end{bmatrix} + \begin{bmatrix} 0 \\ 128 \\ 128 \end{bmatrix} \tag{3.2}$$

$$\begin{bmatrix} H \\ S \\ V \end{bmatrix} = \begin{bmatrix} \tan^{-1}\dfrac{C_B}{C_R} \\ \sqrt{{C_R}^2 + {C_B}^2} \\ Y \end{bmatrix} \tag{3.3}$$

3.3.3 Estimation of Sclera Area

Two approaches were used to find potential sclera areas. The first approach was based on the fact that the sclera area is the 'non-skin' area of the eye region. This allows for simple heuristics to be used to classify areas in the image as 'skin' or 'not-skin' as described in [56, 57], and then a binary map of the sclera is assumed to be the inverse of the skin. The first color distance map, for natural illumination, is calculated using:

$$CDM_1 = \begin{cases} 1, & \begin{matrix} R > 95, G > 40, B > 20, \\ \max(\mathrm{R},\mathrm{G},\mathrm{B}) - \min(\mathrm{R},\mathrm{G},\mathrm{B}) > 15, \\ |R - G| > 15, R > G, R > B \end{matrix} \\ 0, & else \end{cases} \tag{3.4}$$

The second color distance map, for flash illuminators, is calculated using:

$$CDM_2 = \begin{cases} 1, & \begin{matrix} R > 220, G > 210, B > 170, \\ \max(\mathrm{R},\mathrm{G},\mathrm{B}) - \min(\mathrm{R},\mathrm{G},\mathrm{B}) > 15, \\ |R - G| \leq 15, R > B, B > G \end{matrix} \\ 0, & else \end{cases} \tag{3.5}$$

Then, the sclera map is calculated using the two color distance maps:

$$S_1(x,y) = \begin{cases} 1, & CDM_1(x,y)\ OR\ CDM_2(x,y) = 0 \\ 0, & else \end{cases} \tag{3.6}$$

A second potential sclera map is designed based on the fact that the sclera area is the "white" area of the eye. In other words, the hue of the sclera area should have low hue (about bottom 1/3), low saturation (bottom 2/5), and high intensity (top 2/3). Therefore, the following heuristic is developed:

$$S_2(x,y) = \begin{cases} 1, & \begin{matrix} if\ H(x,y) \leq th_h \\ and\ S(x,y) \leq th_s \\ and\ V(x,y) \geq th_v \end{matrix} \\ 0, & else \end{cases} \tag{3.7}$$

With the thresholds calculated using:

$$th_h = arg\left\{t \left| \min \left| \sum_{x=1}^{t} p_h(x) - T_h \right| \right.\right\},$$
$$th_s = arg\left\{t \left| \min \left| \sum_{x=1}^{t} p_s(x) - T_s \right| \right.\right\}, \quad (3.8)$$
$$\text{and } th_v = arg\left\{t \left| \min \left| \sum_{x=1}^{t} p_v(x) - T_v \right| \right.\right\}.$$

Here $p_h(x)$ is the normalized histogram of the hue image, $p_s(x)$ is the normalized histogram of the saturation image, $p_v(x)$ is the normalized histogram of the value image, and $S_2(x, y)$ is the binary sclera map. In this way, we generate two binary maps $S_1(x, y)$ and $S_2(x, y)$. The thresholds T_h, T_s, and T_v are 1/3, 2/5, and 1/3 respectively. Morphological operations are applied to the two binary maps to remove isolated pixels, and small regions of contiguous pixels.

3.3.4 Convex Hull of Estimated Sclera

The convex hull of each of these sclera representations is calculated. The convex hull is the minimal convex set of points that contains the entire original set [58]. It can be visualized as the boundary of the set of points that contains all of the points, without requiring a concave segment, or as if one were stretching an elastic band around the set of points.

3.3.5 Color-Based Sclera Region Estimation Scheme

The best estimate of the sclera is determined by dividing each individual mask into two sections — left and right of the detected pupil center. The final representation is created using the individual portions that are the most homogenous, by minimizing the standard deviation of the pixels in the region.

$$r = arg\left\{ i \left| \min \sum_{(x,y)\in S_i} (I(x,y) - m_i)^2 \right. \right\}, \tag{3.9}$$

where r is the region to be retained, S_i is the i[th] region, $I(x,y)$ is the intensity image, and m_i is the mean intensity of the i[th] region. This process is illustrated in Figure 3.2. Then the convex hull of the estimated region is calculated.

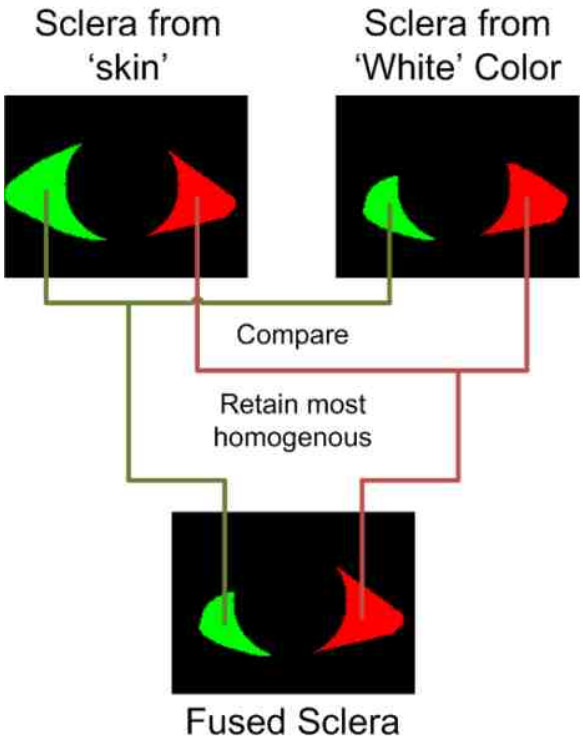

Figure 3.2 Fusing the sclera representations

3.3.6 Iris Segmentation

In this research, we focused on sclera recognition using frontal-gaze eyes. To improve the segmentation speed, the pupil and iris regions are simply modeled as circular boundaries and typical circular iris segmentation methods were used [6, 7, 39, 43, 46, 50, 59-61], and the convex hull of the iris is removed from each of the estimated sclera representations.

Specifically, the pupil and iris regions are segmented using a greedy angular search to find the pupil and iris boundaries, and using a least squares circle fitting algorithm to fit a circle to the detected boundaries. An overlapping greedy angular search is performed on the edge detected image, which can accurately detect the pupil boundaries regardless of gaze direction and eyelid/eyelash occlusion. The algorithm searches along the radial direction at a pre-defined set of angles to estimate the pupil boundaries, and then iteratively maps the highest edge value along the angular direction for $\pi/2$ radians for each of these starting angles.

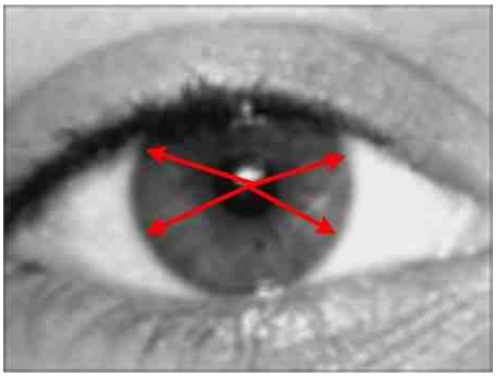

Figure 3.3 Finding the search start points

Starting at the estimated center of the pupil, the algorithm searches along a radial direction for the highest edge value within some radial length range, Eq. 3.10:

$$(u, v) = arg\left\{(x, y) \,\middle|\, \max \mathrm{S}(x, y), with \ \arctan\left(\frac{y-y_0}{x-x_0}\right) = \theta\right\}. \tag{3.10}$$

Here, $S(x, y)$ is the edge detected image, (x_0, y_0) is the estimated pupil center, and θ is the angular search direction. Then, using this detected point as the start of the search, the algorithm iteratively searches for the highest edge value along the angular direction, constraining the possible outcomes to the next pixel in the defined angular direction and its two nearest neighbors along the radial dimension, Eq. 3.11.

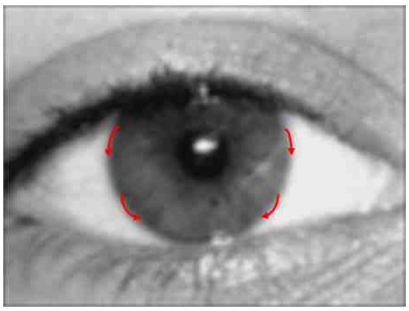

Figure 3.4 Searching along the radial direction

$$(u,v) = arg\left\{(x,y)\left|\max \mathrm{S}(x,y), \begin{matrix} x = x_0 + r\cos\theta, \\ y = y_0 + r\sin\theta, \\ r^{'} - 1 \le r \le r^{'} + 1 \end{matrix}\right.\right\}, \tag{3.11}$$

where $r^{'}$ is the previous iteration's radius. The search continues for $\pi/2$ radians, and combine the aggregate results for all initialization orientations. The final result will be an image with each pixel's value equal to the number of individual radial searches that include that particular pixel. The "majority vote" approach is used to determine which pixels to include in the final iris boundary mask, eliminating pixels that were not commonly 'found' in the search. Figure 3.5 shows the aggregate results of 5 of these individual searches for pupil detection.

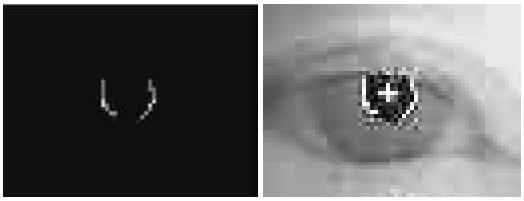

Figure 3.5 The aggregate of 5 individual radial searches,
and the result superimposed on the original image

A least-squares circle is fit to the detected pixels using Kasa's least squares circle fitting algorithm [62].

3.3.7 Iris and Eyelid Refinement

The top and bottom boundaries of the fused sclera region are used as initial estimates of the sclera boundaries, and a polynomial is fit to each boundary. Using the

top and bottom portions of the estimated sclera region and the preliminary iris boundary as guidelines, the upper eyelid boundary, lower eyelid boundary, and iris boundary are then refined using the Fourier active contour method [7].

A radial derivative, centered on the detected pupil center, is calculated using Eq. 3.12.

$$D_{\emptyset}(x,y) = \sum_{i=-n}^{n} w_i I(r+i,\theta), \tag{3.12}$$

$$\emptyset = \tan^{-1}\frac{y-y_0}{x-x_0},$$

$$r = \sqrt{(x-x_0)^2 + (y-y_0)^2}, \tag{3.13}$$

$$w_i = sgn(i)(4-|i|)\,,$$

Where $(x_0, y_0)$is the detected pupil center, $D_{\emptyset}(x,y)$ is the directional derivative, $I(r,\theta)$ is the original grayscale intensity image using radial coordinates, and $2n+1$ is the radial filter length. Figure 3.6 shows an example radial derivative.

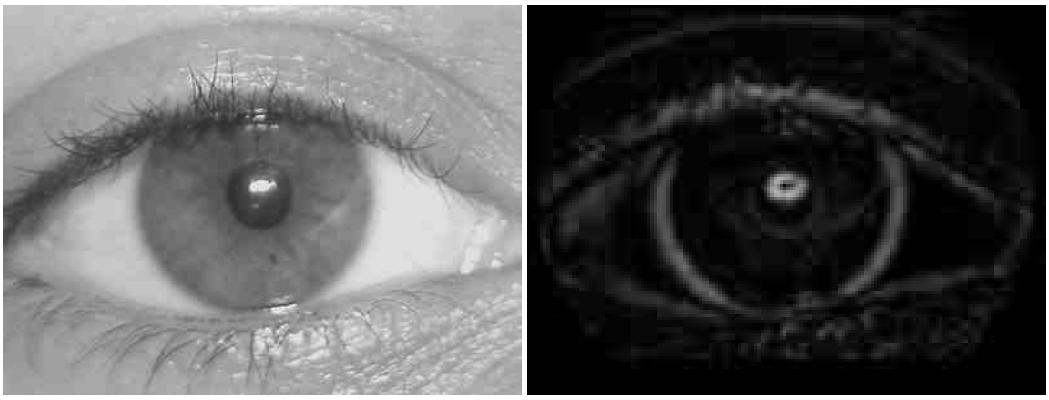

Figure 3.6 The original intensity image and the radial derivative

Then, a new derivative region-of-interest, ROI, image is created by normalizing the radial derivative image along the estimated eyelid boundary with respect to the eyelid boundaries derivative, using Eq. 3.14.

$$
\begin{aligned}
D_{\emptyset Norm}(x,y) &= D_{\emptyset}[x_n(x,y), y_n(x,y)], \\
x_n(x,y) &= \left\lfloor \left(y - \frac{Y}{2}\right)\cos\left(e_{tan}(x)\right) + e_x(x) \right\rfloor \\
y_n(x,y) &= \left\lfloor \left(y - \frac{Y}{2}\right)\sin\left(e_{tan}(x)\right) + e_y(x) \right\rfloor \\
x &= 1 \ldots N, y = 1 \ldots Y
\end{aligned}
\tag{3.14}
$$

Where, $e_{tan}(x)$ is a function that returns the evaluated tangent angle of the nth pixel of the pupil boundary, $e_x(n)$ is a function that returns the evaluated x-coordinate of the nth pixel of the pupil boundary, $e_y(n)$ is a function that returns the evaluated y-coordinate of the nth pixel of the pupil boundary, $D_{\emptyset Norm}(x,y)$ is the normalized directional derivative, $Y/2$ is the distance to be normalized around the eyelid boundary, and N is the length of the eyelid boundary. Thus, the new normalized derivative has the estimated eyelid boundary as the middle row of the image, and the remaining pixels sampled along the tangent lines of the estimated boundary. The region of interest is shown as the red box in Figure 3.7, with the green line showing the original estimated eyelid from the sclera estimation.

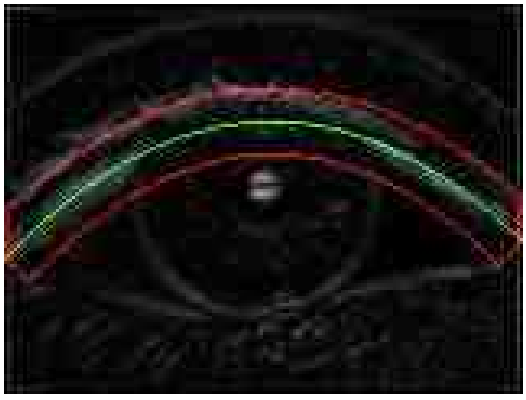

Figure 3.7 The eyelid region-of-interest

Figure 3.8 The optimal path through the eyelid ROI

The iris and eyelid boundaries are refined using a Fourier representation, similar to the one implemented in [7]. A dynamic programming approach [58] is used to determine a globally maximal path, p_x, through $D_{\emptyset Norm}(x, y)$ (the red line in Figure 3.8). Then, this path is described by computing the Fourier expansion of the data (Eq. 3.15), truncating the number of coefficients used to describe the path, and re-computing the final boundary from the truncated coefficients (Eq. 3.16).

$$C_k = \sum_{x=0}^{N-1} p_x e^{-2\pi ikx/N} \tag{3.15}$$

$$P_x = \frac{1}{N} \sum_{k=0}^{M-1} C_k e^{2\pi ikx/N} \tag{3.16}$$

Where N is length of the path, p_x, M is the number of retained coefficients, and P_x is the final path, expressed in the coordinates of the normalized region-of-interest directional derivative. This path must be transformed back to the original coordinate system of the original image, using Eq. 3.17. Figure 3.9 shows an example eyelid boundary after active contour refinement.

$$\begin{gathered} P_x(x', y') = \left\{P_o(x)\cos\left(e_{tan}(x)\right) + e_x(x),\ P_o(x)\sin\left(e_{tan}(x)\right) + e_y(x)\right\} \\ P_o(x) = \left(P_x(x) - \frac{Y}{2}\right) \\ x = 1 \ldots N \end{gathered} \tag{3.17}$$

Figure 3.9 The final eyelid boundary after active contour representation

In a similar fashion, the iris boundary is modeled as a circle, and then refined using the same method as described for the eyelids. The only major difference is that instead of modeling the boundary as a general polynomial, it is modeled as a circle, from the original estimate of the iris boundary. The modified equations required are:

$$f_{iris}(x,y) = \frac{(x-x_0)^2 + (y-y_0)^2}{r^2} \tag{3.18}$$

$$\begin{aligned} D_{\emptyset Norm}(x,y) &= D_{\emptyset}[x_n(x,y), y_n(x,y)], \\ x_n(x,y) &= \left\lfloor \left(y - \frac{Y}{2}\right)\cos\left(i_{tan}(x)\right) + i_x(x) \right\rfloor \\ y_n(x,y) &= \left\lfloor \left(y - \frac{Y}{2}\right)\sin\left(i_{tan}(x)\right) + i_y(x) \right\rfloor \\ x &= 1 \ldots N, y = 0 \ldots Y, \end{aligned} \tag{3.19}$$

where, similar to the previous section, $i_{tan}(n)$ is a function that returns the evaluated tangent angle of the nth pixel of the iris boundary, $i_x(n)$ is a function that returns the evaluated x-coordinate of the nth pixel of the iris boundary, $i_y(n)$ is a function that returns the evaluated y-coordinate of the nth pixel of the iris boundary. Additionally, the calculated eyelid boundaries are used to limit the iris boundary — i.e., the iris mask cannot be above the upper eyelid boundary or vice versa for the lower eyelid boundary. Figure 3.10 to Figure 3.12 show the active contour method as applied to the iris.

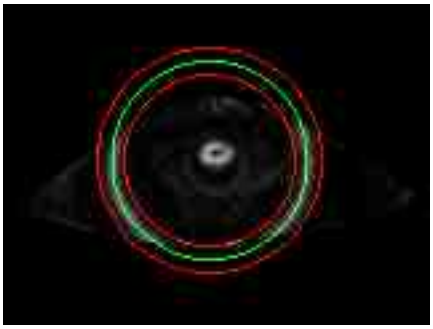

Figure 3.10 The initial estimate of the iris boundary

Figure 3.11 The optimal path through the normalized radial derivative

Figure 3.12 The active contour approach applied to the iris boundary

3.3.8 Creation of the Sclera Mask and Upsampling the Sclera Mask

Finally, after having refined the upper and lower eyelids and the iris boundaries, the detected sclera region is segmented. The mask of the segmentation result is upsampled back to the original images size using a simple interpolation method.

Figure 3.13 shows an example of a segmented sclera image — note that there are some areas which are not perfectly segmented. In reality, perfect segmentation of all images is impossible. Therefore, in this research we focused on designing the feature extraction and matching portions of the system so that they are tolerant of segmentation error.

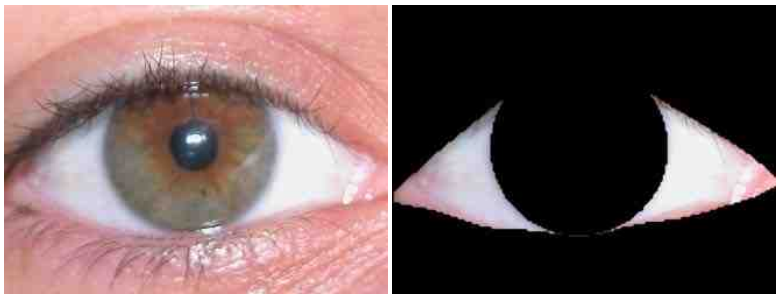

Figure 3.13 A segmented sclera image

3.4 Sclera Segmentation Results

Manual examination of the segmentation results from the UBIRIS database show that 110 images out of 1749 images (6.3% of the images) had noticeable segmentation errors. However for the segmentation results to significantly affect the matching results, very little of the sclera region must be segmented. There were less than 10 images that had segmentation errors where a significant portion of the sclera region was not included in the segmentation region and the matching results would be affected. Some representative results from the sclera segmentation system are presented below. In each image the area detected as sclera is artificially colored red, and the non-sclera regions are colored green, for ease of viewing.

First, some example well-segmented sclera images are presented in Figure 3.14. As described previously in the sclera segmentation system outline, the system aims to produce accurate segmentation results, but borders on under segmenting the sclera region. In Figure 3.15, some example poorly segmented images are presented. In particular, note that a majority of the mis-segmented images are problematic near the lower eyelid boundary. As mentioned previously, the lower eyelid boundary tends to be very difficult to segment due to a similar color between the eyelid and the very vascular sclera region and the level of ‘texture’ that the large amount of vasculature introduces. Additionally, there are several images where there are areas that are defined as sclera that should obviously not be — isolated areas, areas above the pupil, etc.

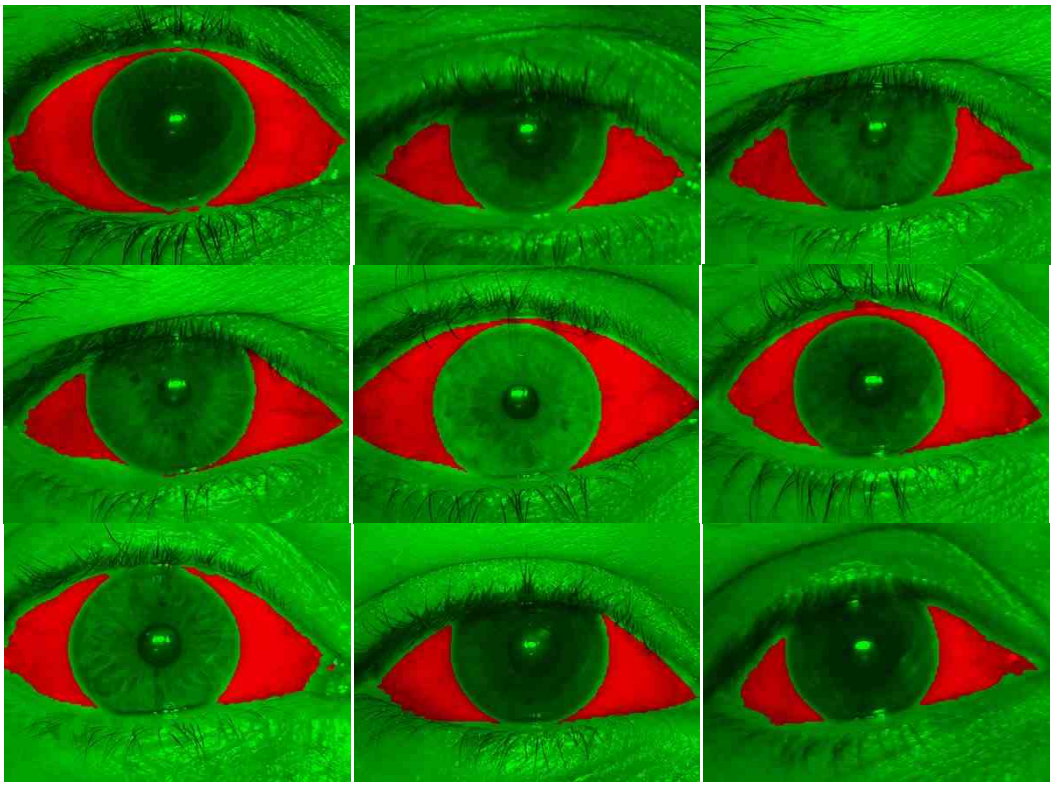

Figure 3.14 Well segmented sclera regions

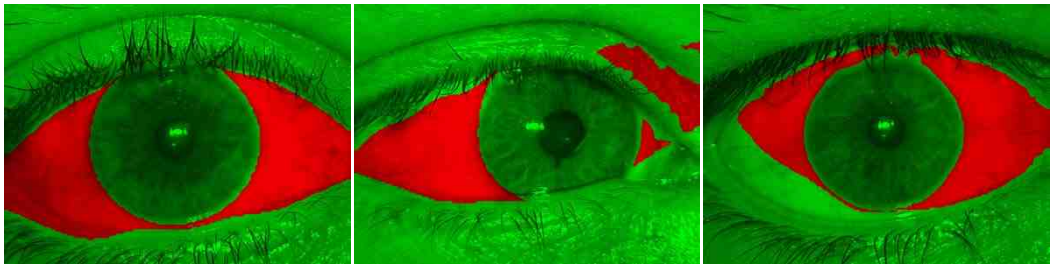

Figure 3.15 Poorly segmented sclera regions

For the left-most image in Figure 3.15, the lower left eyelid boundary was incorrectly segmented — most likely due to the small color differences between the sclera and skin near the lower eyelid boundary. This particular issue is further covered in Section 3.4.1. For the middle image in Figure 3.15, an isolated region non-sclera region was incorrectly segmented as sclera, due to incorrect initial sclera region estimation. Finally, for the right-most image in Figure 3.15, the sclera boundary was over-segmented due to a combination of some error in the initial sclera region estimation coupled with the

active contour following the strongest edge in the region, a vein rather than the lower eyelid boundary. For each of these cases, the sclera segmentation was not ideal, but, as one can see, the majority of the sclera region was segmented.

In each of the above cases, even with the incorrect segmentation, the particular images were still able to be identified. This is accomplished due to the implementation of the matching algorithm. To limit the potential effects of these types of mis-segmented regions, the matching algorithm uses the detected vein patterns in the detected sclera regions to register the test and target descriptors, but matches are only computed for those descriptors in areas that are in common between the two descriptors. So, for the cases where there are erroneous sclera regions selected, the 'vein patterns' detected in these regions will only potentially affect the matching results if both the test and target descriptors both include these mis-segmented images. This allows for the segmentation algorithm to be more generalized and less restrictive, and still not unduly affect the overall matching results.

3.4.1 Challenging Cases for Sclera Segmentation

In this work, the major challenging cases for sclera segmentation were images where there was very little sclera region to be segmented and properly segmenting the lower eyelid boundary. Figure 3.16 shows an example image with very little sclera region to be segmented.

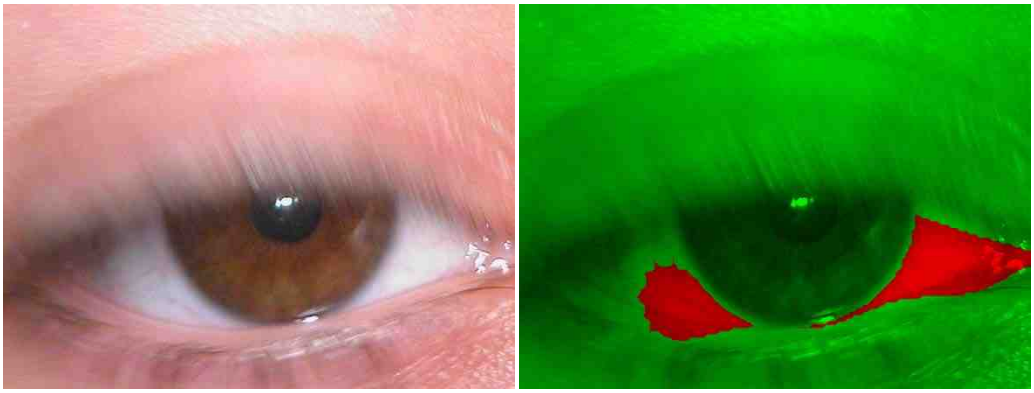

Figure 3.16 An example image with very little sclera region to segment

Figure 3.17 shows an image with a poorly segmented lower eyelid boundary due to a small color difference between the sclera and eyelid. In Figure 3.17, the bottom image is a color gradient image, where higher values show larger Euclidean differences between that pixel's RGB color vector and its neighbor pixel's RGB color vector. This image shows that the color differences between the lower eyelid and sclera are very small, due to the low intensity of the pixels in that region in the color gradient image.

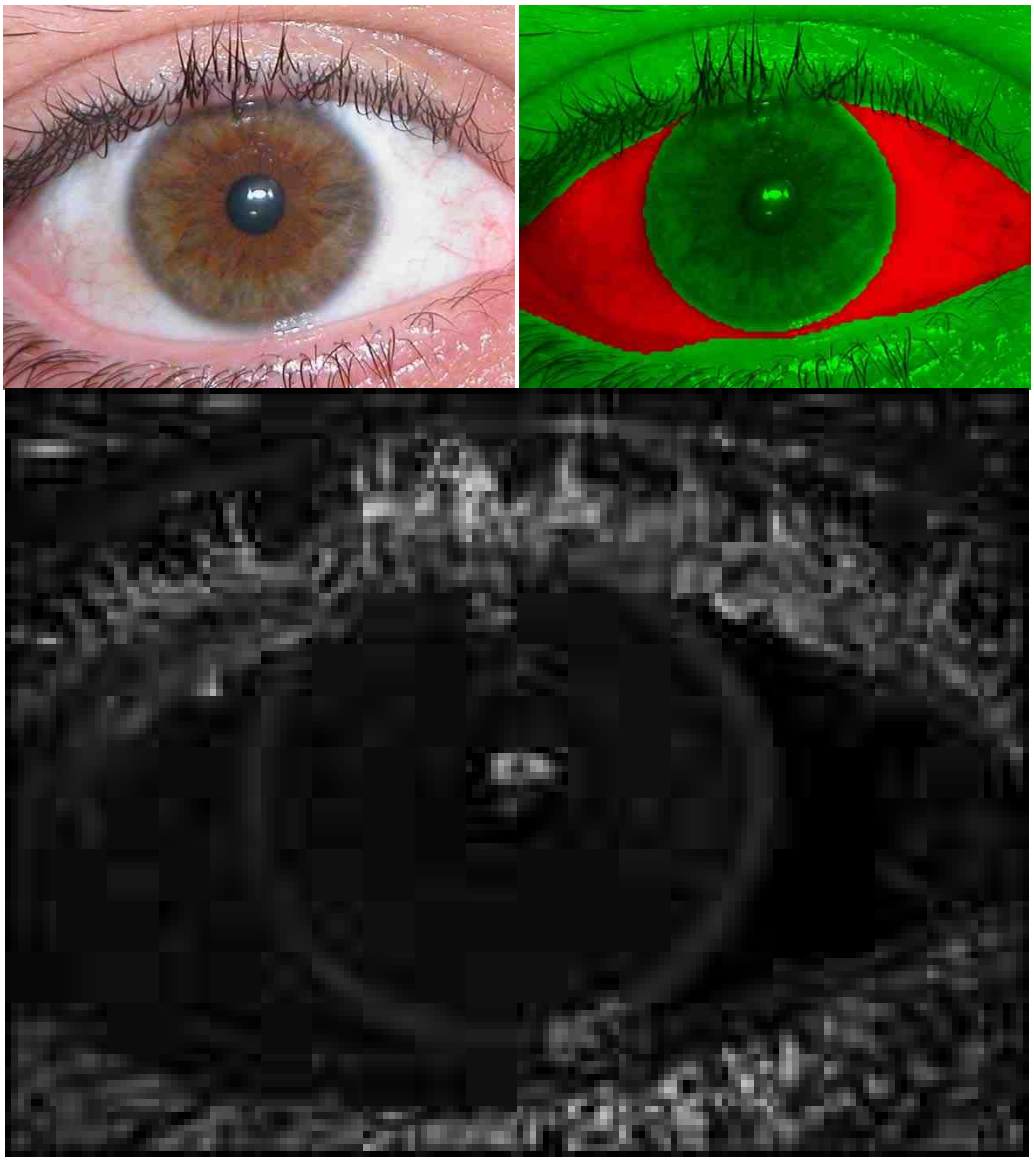

Figure 3.17 An example image that is difficult to segment due to small color differences

3.5 Summary

In comparison to previous sclera segmentation algorithms, the proposed system presents a fully automated sclera segmentation system that can accurately segment the sclera region using color images, does not require training, and does not include any manual intervention. It uses a color-based system to estimate the sclera region, and uses

this initial estimate to then refine the boundaries adjacent to the sclera (the eyelids and iris) using an active contour approach, which has been implemented for any general contour.

The experimental results show that the proposed system can accurately segment the sclera region. Manual inspection of the segmentation results of the entire UBIRIS database showed that roughly 6% of the images had noticeable segmentation errors. However, there were very few (less than 1%) segmentation errors.

4. FEATURE ENHANCEMENT AND EXTRACTION

4.1 Review of Image Enhancement Techniques

Two general image enhancement techniques that are frequently used to perform preliminary image enhancement are contrast stretching and histogram equalization.

4.1.1 Contrast Stretching

Contrast stretching is a linear transformation that increases the dynamic range of an image [63]. Typically, this is done such that the lowest intensity value in the input image is mapped to an output value of '0', and the highest intensity value in the input image is mapped to an output value of '1'. Using this type of simple contrast stretching normalizes the range of pixel values, but cannot guarantee consistent results. Examples of cases where this simple type of contrast stretching would be inadequate would be if the input image already includes saturated upper and lower pixel values or if there is a small outlier saturation region. Figure 4.1 shows a low contrast image and its histogram. Note how the distribution of pixel values is clustered around 50. Figure 4.2 shows the low contrast image after contrast stretching and its histogram. The histogram of the contrast stretched image is shifted to the right and stretched to encompass the entire range, as compared to the original histogram, but it retains the same general shape as the original. For this work, simple contrast stretching is not adequate, by itself, for the feature enhancement because the features to be enhanced are local, and contrast stretching works globally on the image. However, we used contrast stretching as a preliminary image enhancement step before segmentation.

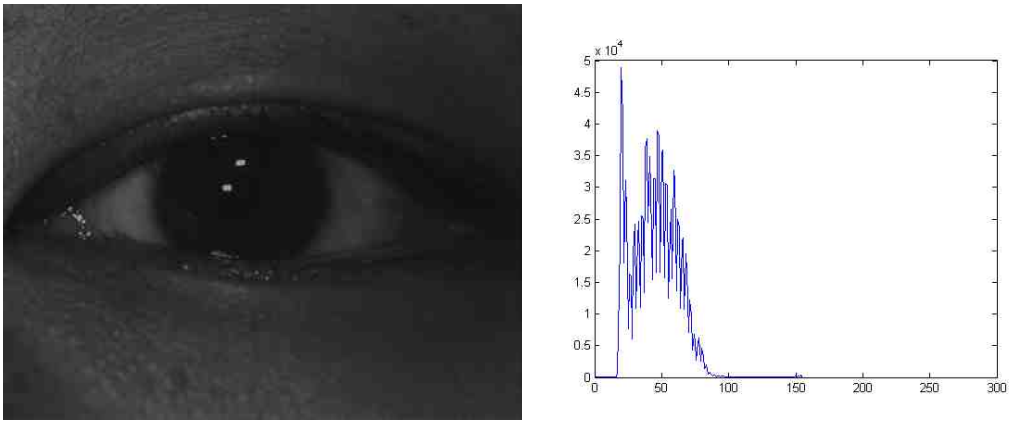

Figure 4.1 A low contrast image, and its corresponding histogram

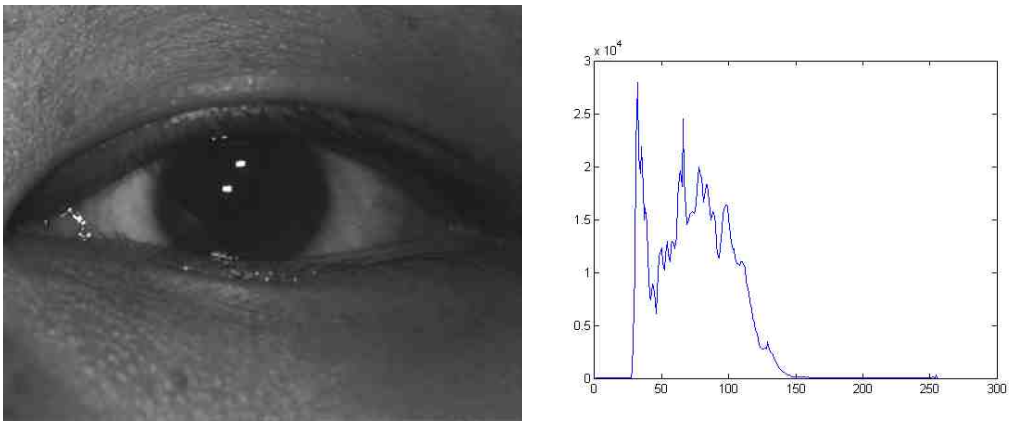

Figure 4.2 The low contrast image after contrast stretching, and its histogram

4.1.2 Histogram Equalization

Histogram equalization is an intensity transformation that transforms the distribution of the pixels intensity values into a uniform, or nearly uniform, distribution [63]. Specifically, this transformation treats the pixel values in the image as a random variable, and looks to apply a transformation that transforms the unknown distribution to a uniform one. Figure 4.3 shows the low contrast image after histogram equalization and its histogram. Note that the resultant histogram is much more evenly distributed than the original images. Similarly to contrast stretching, globally applied histogram equalization is not adequate for the sclera vein enhancement due to its global operation on the image.

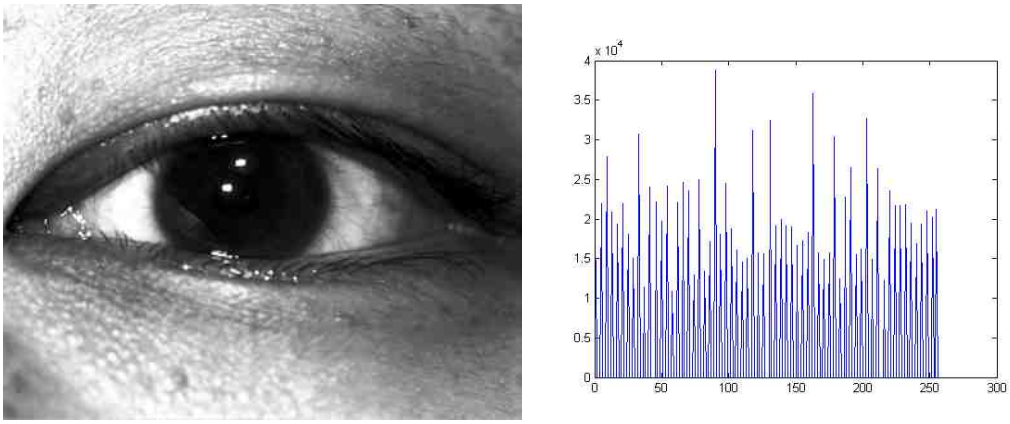

Figure 4.3 The low contrast image after histogram equalization, and its histogram

4.2 Review of Previous Sclera Feature Enhancement and Extraction Techniques

In [25], Derakhshani *et al.* first described a vein extraction and enhancement technique. In this work, the authors first enhanced the green colorplane of the image using a contrast-limited adaptive histogram equalization technique (CLAHE). CLAHE is a histogram equalization technique that enhances small regions, or 'tiles', of the image separately and uses bilinear interpolation to limit artificially introduced boundaries between adjacent tiles [64]. The authors then use a line and curve detection method, as described in [65] to enhance the veins, and then use a region growing approach as outlined in [21] to binarize the vein image.

In [27], Derakhshani and Ross also used the CLAHE technique to enhance the green colorplane of the sclera images. For feature extraction, the authors downsampled the image to 100x200 pixels, and used the discrete Cohen-Daubechies-Feauveau 9/7 Wavelet transform (CDF 9/7) to transform the sclera image into the wavelet domain. The authors then used the first 512 wavelet coefficients as the sclera images' feature vector.

Most recently, in [28], Crihalmeanu *et al.* also used the CLAHE technique to enhance the green colorplane of the sclera image, and used the same line and curve detection/enhancement method that was used in the first work.

Note that all of these enhancement and extraction schemes proposed specifically assume that the sclera vein patterns are one-dimensional and that the vein branch points are useful features for matching. However, as shown earlier, this sclera vein patterns are not one dimensional, and in many cases, this choice of features will significantly reduce the systems accuracy, in a realistic operational environment.

4.3 Proposed Sclera Feature Enhancement and Extraction Method

The proposed sclera feature enhancement and extraction method incorporates a Gabor filter-based vein enhancement method, and a novel line descriptor to extract and describe the vein structure in the presence of noise and deformation.

4.3.1 Gabor Filter Vein Enhancement

Figure 3.13 shows the segmented sclera area, which is highly reflective and hard to be accurately focused in the image acquisition process. As a result, the sclera vascular patterns are often blurry and/or have very low contrast. It is important to enhance the vascular patterns before feature extraction. In [66], Daugman shows that the family of Gabor filters, which are Gaussian weighted sinusoids, are good approximations of the vision processes of the primary human visual cortex. Because the vascular patterns could have multiple orientations, in this research, a bank of directional Gabor filters (Figure 4.4) is used for vascular pattern enhancement:

$$G(x, y, \vartheta, s) = e^{-\pi\left(\frac{(x-x_0)^2+(y-y_0)^2}{s^2}\right)} e^{-2\pi i\left(\cos\vartheta(x-x_0)+\sin\vartheta(y-y_0)\right),} \quad (4.1)$$

where (x_0, y_0) is the center frequency of the filter, s is the variance of the Gaussian, and ϑ is the angle of the sinusoidal modulation. For this work, only the even filter was used for feature extraction of the veins. Experimentally, the even filters response was determined to adequately identify the veins, so the odd filter was not used to reduce the computational time.

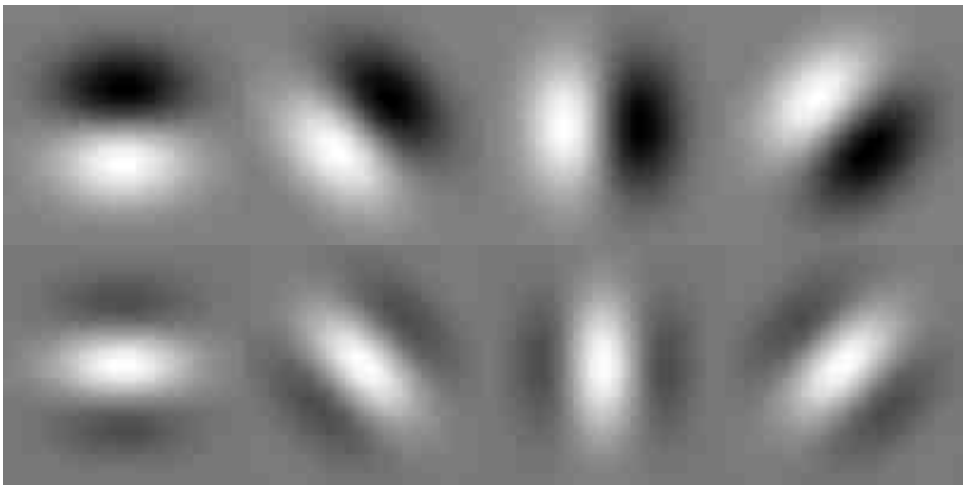

Figure 4.4 An example image of a Gabor filter bank with 4 directions. The top image is an even filter bank, and the bottom is an odd filter bank.

The image is first filtered with Gabor filters with different orientations and scales:

$$I_F(x, y, \vartheta, s) = I(x, y) * G(x, y, \vartheta, s) \tag{4.2}$$

where $I(x, y)$ is the original intensity image, $G(x, y, \vartheta, s)$ is the Gabor filter, $I_F(x, y, \vartheta, s)$ is the Gabor filtered image at orientation θ and scale s. Both θ and S are determined by the desired features to be extracted in the database being used. For example, in the UBIRIS database, the typical vein width was around 4 pixels wide, so the filters were constructed with a filter bandwidth of 3, 4, and 5 pixels, respectively. Similarly, it was determined experimentally that, for the UBIRIS database, four angular orientations were adequate for accurate vein enhancement and extraction. In a practical system, these parameters would be set by examining exemplar data All the filtered images are fused together to generate the vein-boosted image, $F(x, y)$:

$$F(x, y) = \sqrt{\sum_{\vartheta \in \theta} \sum_{s \in S} \left(I_F(x, y, \vartheta, s)\right)^2} \tag{4.3}$$

Figure 4.5 shows the results before and after Gabor enhancement of a sclera vein pattern. In Figure 4.5(a), the vein structure in the sclera region is very difficult to see, however, in Figure 4.5(b), after Gabor enhancement but before thresholding, the vein structure is clearly visible.

An adaptive threshold, based on the distribution of filtered pixel values, is used to determine a threshold to binarize the Gabor filtered image, using Eq. 9.

$$B(x,y) = \begin{cases} 1, & F(x,y) > \underset{t}{\operatorname{argmin}} \left\{ t \left| \sum_{x=1}^{t} p_{edge}(x) - T_p \right| \right\} \\ 0, & else \end{cases}, \tag{4.4}$$

where $B(x,y)$ is the binary vein mask image, $F(x,y)$ is the vein-boosted image, and $p_{edge}(x)$ is the normalized histogram of the non-zero elements of $F(x,y)$. In practice, the zero elements of the filtered image are a significant portion of the image, and in general, the vascular patterns have higher magnitude than the background. Therefore, T_p is selected to be 1/3. Figure 4.5(c) shows a representative result after thresholding

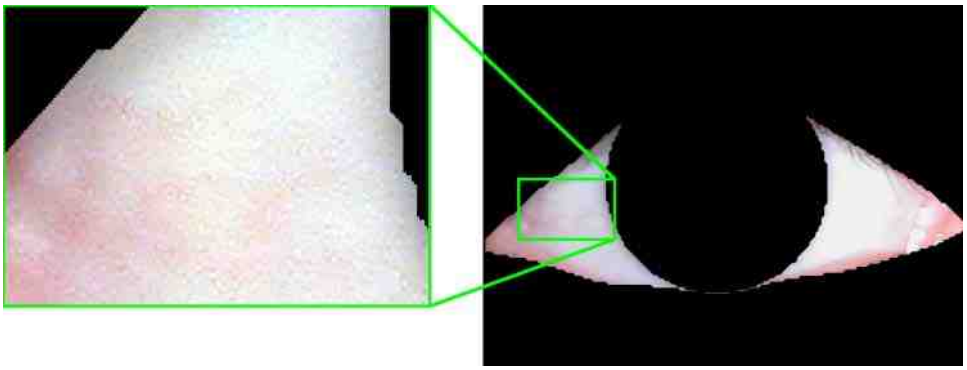

(a) segmented sclera region

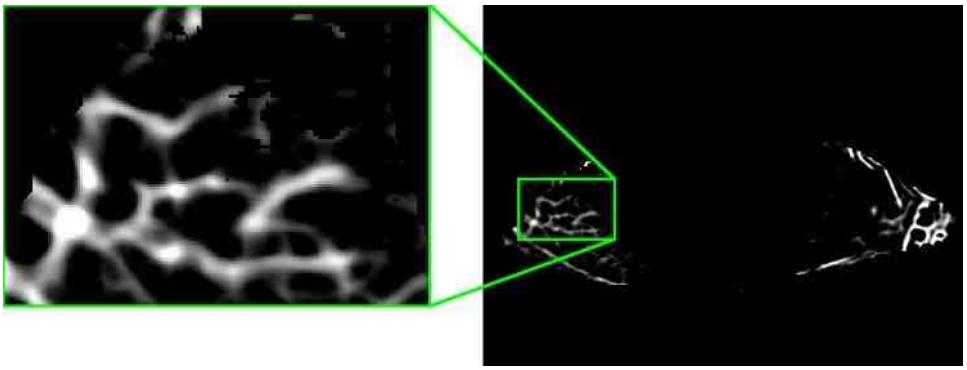

(b) after Gabor enhancement (vein-boosted image)

Figure 4.5 (a-d) Vein patterns – before and after Gabor enhancement

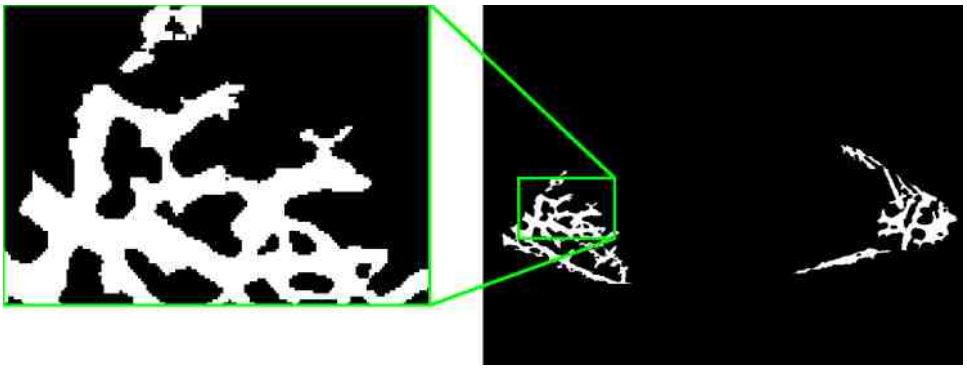

(c) after thresholding (binary vein image)

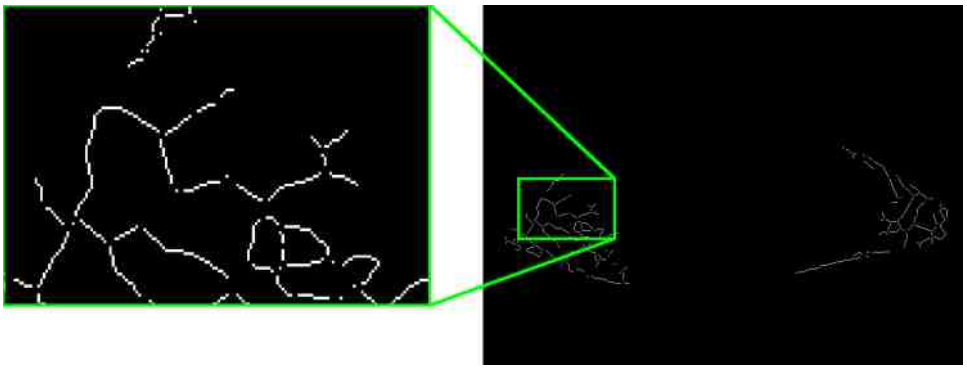

(d) after morphological operations (binary vein skeleton)

Figure 4.5 (a-d) Continued

Then, small simply connected regions in the binary mask image are removed if their volume is below a threshold, as calculated below.

Algorithm for adaptive removal of small connected regions:

- Label the connected binary regions in the veinMask image
- Sort the veinMask elements in order of increasing region size
- Calculate the slope of the set of ordered veinMask elements, $veinMaskEl$
  - $slope(n+1) = veinMaskEl(n) - veinMaskEl(n+1)$
- Calculate the area threshold
  - $sizeThresh = veinMaskEl\left[\text{argmin}_t\left(\left|\sum_{n=1}^{t} slope(n) - .2 * \sigma_{slope\ (n)}\right|\right)\right]$
- Remove elements with size less than calculated size threshold

4.3.2 Vascular Pattern Extraction: Line Segment Descriptor

Due to physiological status of a person (for example, fatigue or non-fatigue, eye irritation, etc.), the vascular patterns could have different thicknesses at different times, due to the dilation and constriction of the veins. Therefore, vein thickness is not a stable pattern for recognition. In addition, some very thin vascular patterns may not be visible at all times or in all situations. In this research, binary morphological operations are used to thin the detected vein structure down to a single-pixel wide skeleton, and to remove the branch points. This leaves a set of single-pixel wide lines that represents the vein structure. Figure 4.5(d) shows the vein skeleton after binary morphology. These lines are then recursively parsed into smaller segments. This is done until the line's maximum size ensures that the line segments are nearly linear, a property that is useful in feature extraction. In this work, the lines were parsed down to a size of 5 pixels. This small line segment size is small enough, in comparison to the matching distance, that the specific starting location of the line segment does not pose a significant cause of error for matching. For each segment, a least-squares line is fit to each segment.

These line segments are then used to create a template for the vein structure. The segments are described by three quantities – the segments angle to some reference angle at the pupil center, the segments distance to the pupil center, and the dominant angular orientation of the line segment. The total descriptor for the sclera vein structure is the set of all of the individual segments' descriptors. Note that this implies that, while each segments descriptor is of a fixed length, the overall descriptor for a sclera vein structure can vary. Figure 4.6 shows a visual description of the descriptor.

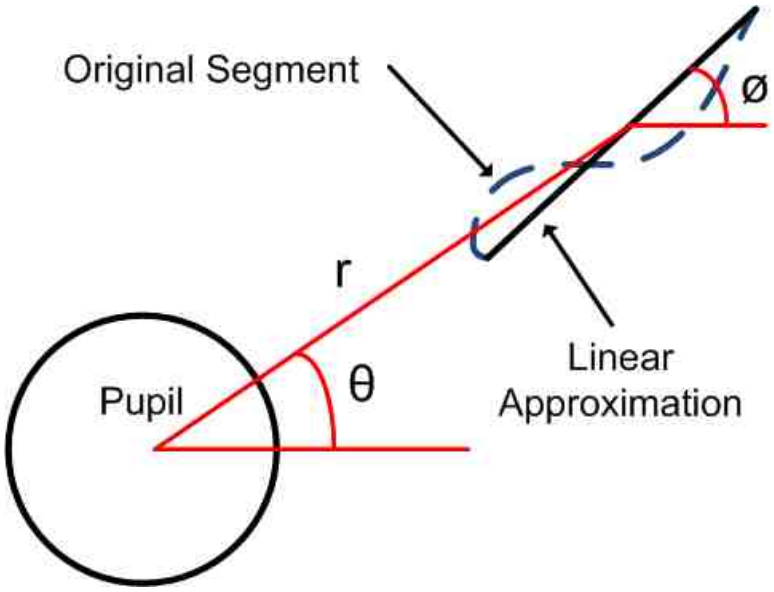

Figure 4.6 The sketch of parameters of segment descriptor

The descriptor is $S = (\theta \quad r \quad \emptyset)^T$. The individual components of the line descriptor are calculated as:

$$\theta = \tan^{-1}\left(\frac{y_l - y_p}{x_l - x_p}\right),$$
$$r = \sqrt{(y_l - y_p)^2 + (x_l - x_p)^2}, \tag{4.5}$$
$$\text{and } \emptyset = \tan^{-1}\left(\frac{d}{dx} f_{line}(x)\right),$$

Here $f_{line}(x)$ is the polynomial approximation of the line segment, (x_l, y_l) is the center point of the line segment, (x_p, y_p) is the center of the detected pupil, and S is the line descriptor. Additionally, the pupil center, (x_p, y_p), is stored with all of the individual line descriptors.

4.4 Sclera Feature Enhancement and Extraction Results

4.4.1 Challenging Cases in Sclera Feature Extraction and Enhancement

In Figure 4.7, we show an example case where the sclera region is out of focus, and therefore the sclera vein pattern cannot be properly and reliably extracted.

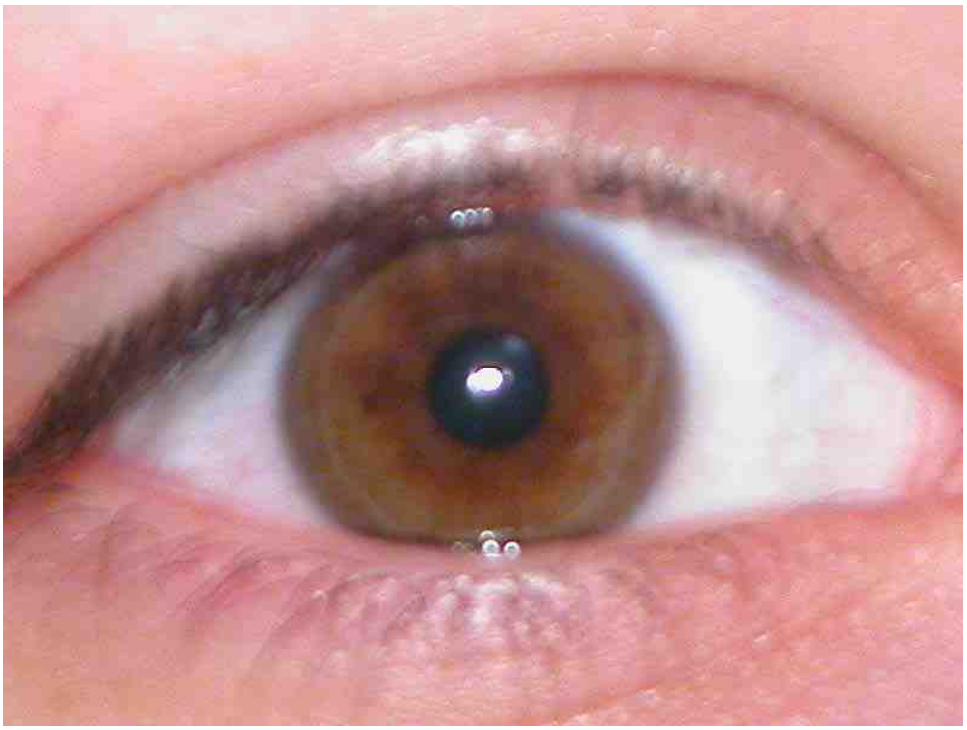

Figure 4.7 An example image with very poor focus that cannot properly extract the vein patterns

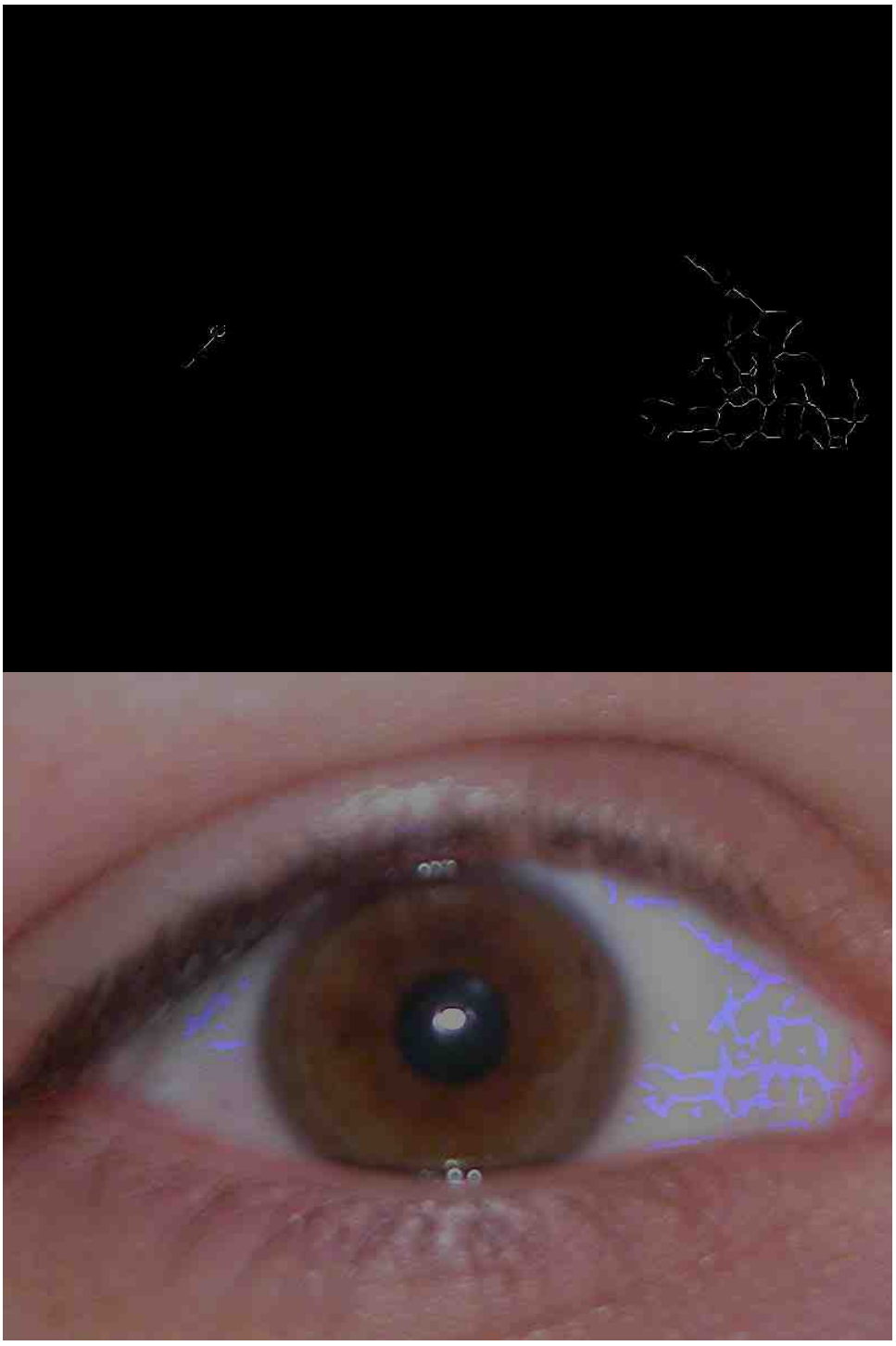

Figure 4.7 Continued

In Figure 4.8 we show an example image with a large area of the sclera that is saturated, and therefore cannot extract the sclera patterns.

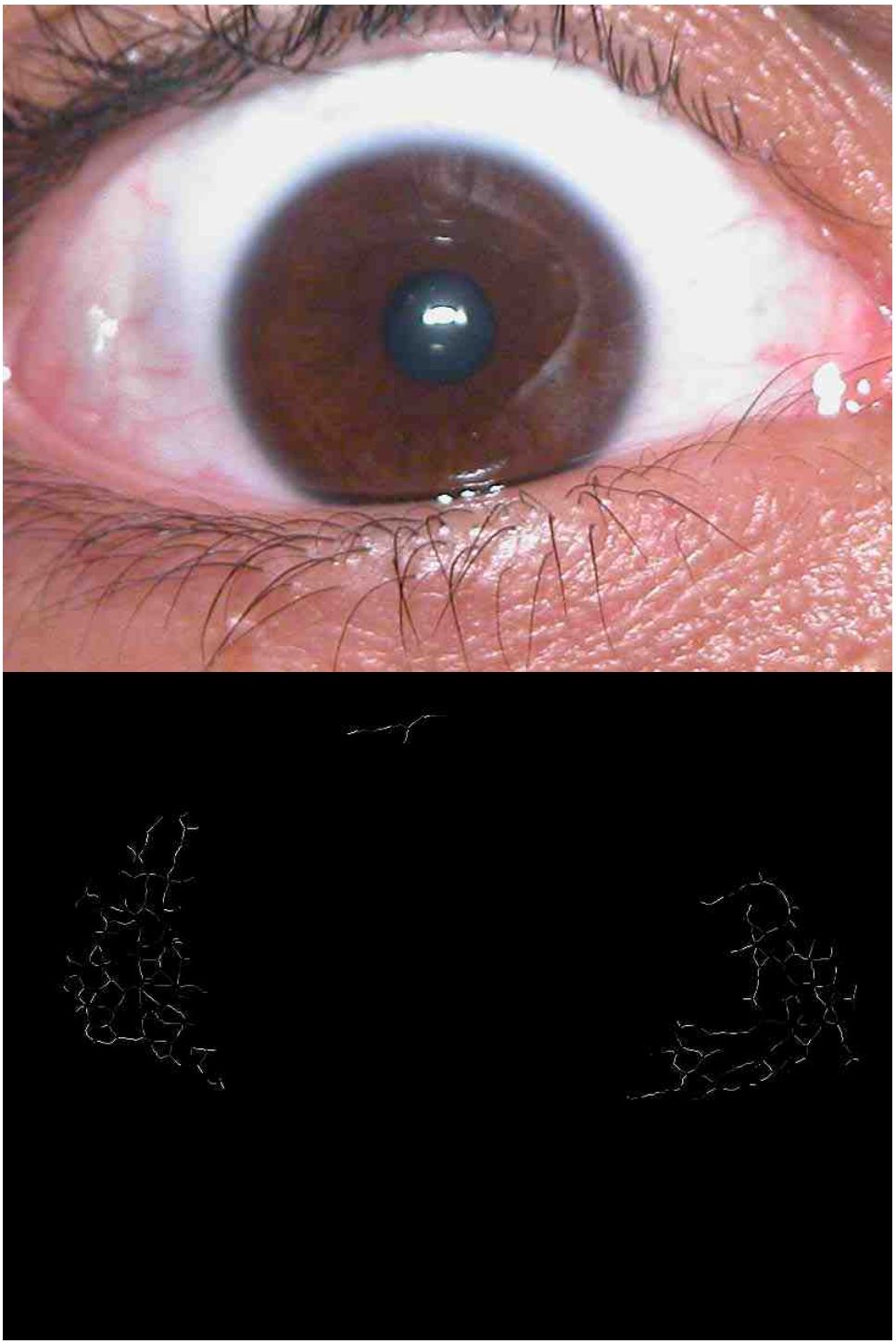

Figure 4.8 An image with a large saturated region in the sclera

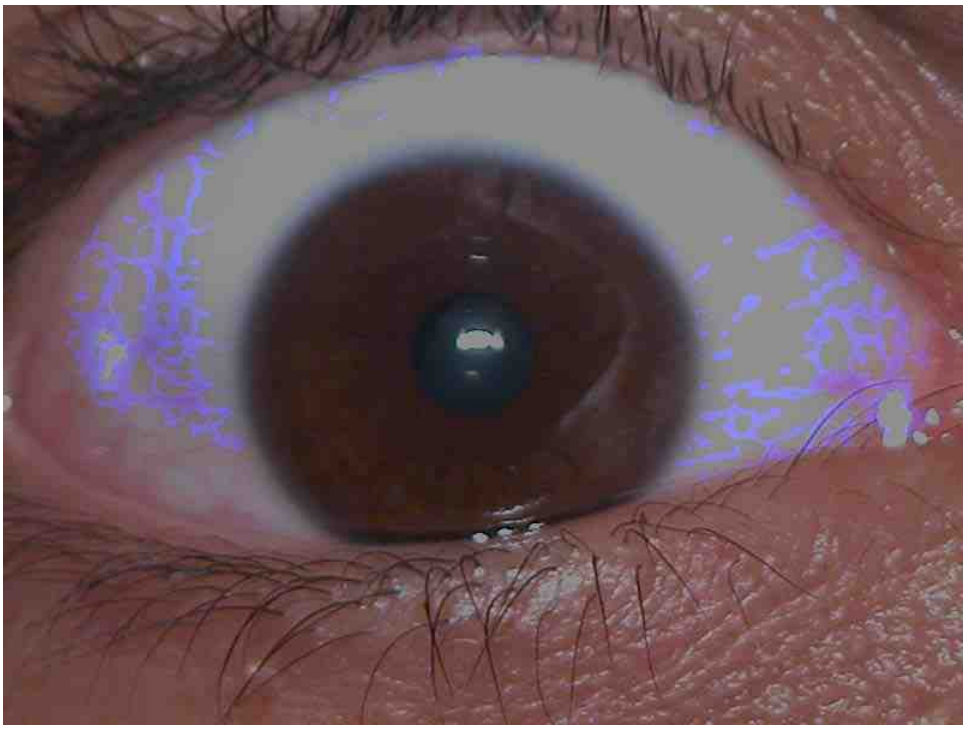

Figure 4.8 Continued

4.5 Summary

In this section, a Gabor filter-based method is proposed that can extract the vein patterns from the sclera images. The Gabor enhanced images are thresholded using a variable threshold, and the resultant binary image is thinned using morphological operations. Finally, a descriptor is created from the extracted linear vein structure to be stored and used for future matching.

The proposed system can robustly extract the vein pattern from non-ideal-quality sclera images. In comparison to previous sclera vein pattern enhancement and extraction techniques, the proposed system is completely automated and does not require any training or manual intervention. Most importantly, the proposed system presents a descriptor for the sclera vein pattern that is discriminating and unique, but can also describe the vein patterns in the presence of the previously mentioned multi-layered, non-linear deformation that the sclera vein patterns exhibit.

5. SCLERA MATCHING

The proposed sclera matching method uses a RANSAC-type registration algorithm to register the sclera vein descriptors, and the proposed sclera template matching method. The proposed sclera matching method is capable of matching the sclera vein patterns even in the presence of noise and deformations.

5.1 Review of General Matching Schemes

Many matching schemes have been proposed and used for previous biometric and pattern recognition applications. Some historical examples of matching schemes are presented, along with justification for their use or disuse.

5.1.1 Hamming Distance

Hamming distance is a distance measure for binary strings that measures the amount of similarity between two strings by measuring the number of bits that must be changed to make the two strings equivalent [67]. It is a common distance metric for biometrics, for instance Daugman's iris recognition algorithms. However, for this work, it is not used, because the feature vectors used are not binary.

5.1.2 Euclidean Distance

Euclidean distance (Eq. 5.1) is the distance between two vectors, and is commonly used as a simple metric for how similar two vectors are [68]. In this work, it is used as the primary measure of how similar two features are.

$$d_{euclid} = \|\boldsymbol{x}_1 - \boldsymbol{x}_2\|^2 = (\boldsymbol{x}_1 - \boldsymbol{x}_2)^T(\boldsymbol{x}_1 - \boldsymbol{x}_2) \quad (5.1)$$

Where d_{euclid} is the Euclidean distance between the vectors, $\boldsymbol{x}_1$ and $\boldsymbol{x}_2$.

5.1.3 Spectral Angle Measure

Spectral angle measure (Eq. 5.2) is a commonly used measure of similarity in hyperspectral and multiple spectrum imaging that measures the similarity between hyperspectral signatures [69].

$$SAM(\boldsymbol{s}, \boldsymbol{s}') = \cos^{-1}\left(\frac{\langle \boldsymbol{s}, \boldsymbol{s}' \rangle}{\|\boldsymbol{s}\|\|\boldsymbol{s}'\|}\right), \quad (5.2)$$

Where $\boldsymbol{s}$ and $\boldsymbol{s}'$ are the spectral signatures of two pixel vectors, $\langle \boldsymbol{s}, \boldsymbol{s}' \rangle = \sum_{l=1}^{L} s_l \, s_l'$, and $\|\boldsymbol{s}\| = [\sum_{l=1}^{L} (s_l)^2]^{\frac{1}{2}}$. However, since our system does not use multiple spectrum information, this measure is not used.

5.1.4 Information Distance

Information distance, or mutual information, (Eq. 5.3) is a measure of the dependence between two random variables [70], and can also be used as a distance metric for feature vectors.

$$I(X;\, Y) = H(X) - H(X|Y) = \sum_{x,y} p(x,y) log\left(\frac{p(x,y)}{p(x)p(y)}\right) \quad (5.3)$$

Where $I(X;\, Y)$ is the mutual information between the two random variables X and Y, $H(X)$ is the entropy of X, $H(X|Y)$ is the conditional entropy of X conditioned on Y, $p(x)$ is the probability that the random variable X takes on value x, $p(y)$ is the probability that the random variable Y takes on value y, and $p(x,y)$ is the joint probability that the random variables, X and Y, take on the respective values x and y.

5.2 Review of Previous Sclera Matching Techniques

In [25], Derakhshani *et al.* propose a multi-level classification system, incorporating both coarse and fine level matching algorithms. They propose to use the course matching to choose some subset of the database for more accurate fine level matching. For the coarse matching, they utilized Hu's affine transformation invariant moments as descriptive features for the binarized vein patterns [26]. In particular, they utilized the 7^{th} moment as the feature, with a reported classification error of 3.47% of all possible matches. For the fine matching, they propose using a minutiae-based matching scheme utilizing the vascular branching points. They do not describe, in detail, their minutiae-based matching algorithm, but report that, with their small database of 6 subjects, they achieved 100% matching accuracy.

In [27], Derakhshani and Ross use a single hidden layer feed forward neural network for matching. The neural network had 512 input nodes, 300 hidden nodes, and 50 output nodes, and used the scaled conjugate gradient algorithm. Note that this network topology is based on the database size (1 output node per user, among other considerations), and as such its computation time will increase dramatically as the database size is increased.

In [28], Crihalmeanu *et al.* report that they used the "cross-correlation between regions of the sclera that do not include the specular reflections from both images." They do not provide any specific information on the particular implementation, and report an EER of ~25%.

5.3 Proposed Sclera Matching Technique

5.3.1 Sclera Template Registration

When acquiring the eye images, the eyelids can have different shapes, the iris location can vary, the pupil size can be different, and the eye may be tilted with respect to the camera. The camera-to-object distance and camera zoom can also vary. All of these factors could affect the size, the location, and the observed patterns of the acquired sclera region in the image. It is important to take these variances into account in a sclera matching algorithm. Therefore, the first step is to perform Sclera region-of-interest, or ROI, registration to achieve global translation-, rotation-, and scaling-invariance. In addition, due to the complex deformation that can occur in the vein patterns, it is desirable to have a registration scheme that is robust and exhaustive, but does not unduly introduce false accepts by over-fitting. Most importantly, as we discussed in Section 1, the sclera vascular patterns deform non-linearly with the movement of the eye, eyelids, and the contraction/dilation of the pupil. As a result, the segments of the vascular patterns could move individually, and this must be accounted for in the registration scheme.

A new method based on a RANSAC-type algorithm was developed to estimate the best-fit parameters for registration between the two sclera vascular pattern descriptors. RANSAC, or random sample consensus, is an iterative model-fitting method that can robustly fit to a model, even given noise [71]. To limit potential false accepts due to over-fitting, the patterns are registered as a set of points – the centers of the line segments that make up the template. The optimal registration used is the one that minimizes the minimum distance between the templates. This reduces artificially introduced false accepts because it does not register the patterns using the same parameters used for matching, so the optimal registration and optimal matching can, and probably will, be different for templates that should not match. For the registration algorithm, it randomly chooses two points – one from the test template, and one from the target template. It also randomly chooses a scaling factor and a rotation value, based on

apriori knowledge of the database. Practically, these parameters would be determined for the specific implementation — expected stand-off distance, capture volume, expected user's motion, etc. For instance, one could calculate the expected variance of the sclera size using the stand-off distance and capture volume. Using these values, it calculates a fitness value for the registration using these parameters. The two descriptors, S_{xi} and S_y, are:

$$S_{xi} = \begin{pmatrix} \theta_{xi} \\ r_{xi} \\ \emptyset_{xi} \end{pmatrix} \text{ and } S_{yj} = \begin{pmatrix} \theta_{yj} \\ r_{yj} \\ \emptyset_{yj} \end{pmatrix} \tag{5.4}$$

The fitness is calculated using the following equations.

First, an offset vector, Eq. 5.5, is created using the shift offset and randomly determined scale and angular offset values.

$$\varphi_0 = \begin{pmatrix} x_o \\ y_o \\ s_o \\ \emptyset_o \end{pmatrix} \tag{5.5}$$

Where:

$$x_o = r_{xi} \cos\theta_{xi} - r_{yj} \cos\theta_{yj}$$
$$y_o = r_{xi} \sin\theta_{xi} - r_{yj} \sin\theta_{yj}$$

The fitness of two descriptors is the minimal summed pairwise distance between the two descriptors given some offset vector, φ_0, calculated using Eq. 5.6.

$$D(S_x, S_y) = \underset{\varphi_0}{\operatorname{argmin}} \widetilde{D}(S_x, S_y, \varphi_0) \tag{5.6}$$

where

$$\widetilde{D}(S_x, S_y, \varphi_0) = \sum_{x_i \in Test} minDist(f(S_{xi}, \varphi_0), S_y) \tag{5.7}$$

Where $f(S_{xi}, \varphi_0)$ is the function that applies the registration given the offset vector to a sclera line descriptor.

$$f(S_{xi}, \varphi_0) = \begin{pmatrix} \cos^{-1}\left(\frac{r_{xi}\cos\theta_{xi} + x_o}{s_o r_{xi}}\right) \\ \frac{r_{xi}\cos\theta_{xi} + x_o}{\cos(\theta_{xi} + \emptyset_o)} \\ \emptyset_{xi} \end{pmatrix} \tag{5.8}$$

Finally, the minimum pairwise distance is calculated using:

$$minDist(S_{xi}, S_y) = \underset{j}{\text{argmin}}\{d(S_{xi}, S_{yj})\} \tag{5.9}$$

With the distance between two points calculated using:

$$d(S_{xi}, S_{yj}) = \sqrt{(x_{xi} - x_{yj})^2 + (y_{xi} + y_{yj})^2} \tag{5.10}$$

where, $Test$ is the set of descriptors in the test template, $Target$ is the set of descriptors in the target template, (x_{xi}, y_{xi}) is the first point used for registration, (x_{yj}, y_{yj}) is the second point, φ_0 is the set of offset parameter values, $f(S_{xi}, \varphi_0)$ is a function that modifies the descriptor with the given offset values, s is the scaling factor, and $\emptyset$ is the rotation value. The algorithm performs some number of iterations, recording the values φ_0 for that are minimal in $D(S_x, S_y)$.

5.3.2 Sclera Template Matching

As discussed previously, it is important to design the matching algorithm such that it is tolerant of segmentation errors. In general, the edge areas of the sclera may not be segmented accurately; therefore the weighting image (Figure 5.1) is created from the common regions of the two registered sclera masks — i.e., only regions that are included in the segmented sclera regions of both images are used for matching. Then, the interior pixels of the mask are set to 1, pixels within some distance of the boundary of the mask to .5, and pixels outside the mask to 0.

This allows for a matching value between two segments to be between 0 and 1, and allows for weighting the matching results based on the segments that are near the mask's boundaries. This reduces the effect of segmentation errors, in particular for under segmentation of the boundary between the sclera and eyelids. For this work, the width of

the boundary of the mask was set to the average width of the lower eyelid boundary in the database, in an attempt to reduce the effect of mis-segmented results near this boundary.

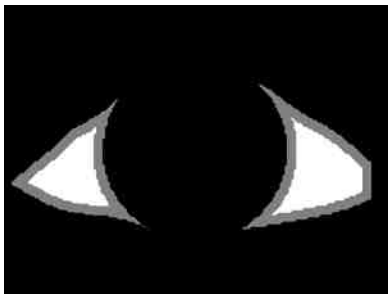

Figure 5.1 The weighting image

After the templates are registered, each line segment in the test template is compared to the line segments in the target template for matches.

$$m(S_i, S_j) = \begin{cases} w(S_i)w(S_j), & \begin{matrix} d(S_i, S_j) \le D_{match} \\ and \\ |\emptyset_i - \emptyset_j| \le \emptyset_{match} \end{matrix} \\ 0, & else \end{cases} \tag{5.11}$$

where S_1 and S_2 are two segment descriptors, $m(S_1, S_2)$ is the matching score between segments S_1 and S_2 , $d(S_1, S_2)$ is the Euclidean distance between the segment descriptors center points (from Eq. 5.10), D_{match} is the matching distance threshold, and $\emptyset_{match}$ is the matching angle threshold. The matching thresholds, D_{match} and $\emptyset_{match}$, were both determined empirically to be 5 pixels and 10°, respectively. $w(S_n)$ is the weight of the n-th segment, and is equal to 1, .5, or 0 if S_n is in the white, grey, or black areas of the mask, respectively.

If there is a non-zero matching score, the segments are removed from future comparisons (one from the test and one from the target templates), and the matching result is recorded. The total matching score, M, is the sum of the individual matching scores divided by the maximum matching score for the minimal set between the test and target template (Eq. 5.12). That is, one of the test or target templates has fewer points,

and thus, the sum of its descriptors weights sets the maximum score that can be attained. This is necessary to normalize the matching scores due to the variation in the number of extracted segments in the descriptors. Specifically, this means that the matching score is a measure of the percentage of matches that are possible for the given pair of templates. If this were not done, images with eyelid occlusion would automatically receive a lower matching score as opposed to those without eyelid occlusion, which is not reasonable for any practical biometric system.

$$M = \frac{\sum_{(i,j)\in Matches} m(S_i, S_j)}{min(\sum_{i\in Test} w(S_i), \sum_{j\in Test} w(S_j),)}, \tag{5.12}$$

where $Matches$ is the set of all pairs of matches, $Test$ is the set of descriptors in the test template, $Target$ is the set of descriptors in the target template.

The proposed matching scheme allows for a multitude of potential changes in the vascular pattern and allows for multiple independent vein patterns to be matched. Additionally, it allows for overlapping vein patterns to be matched even as they change independently, where matching schemes that retain and use the 'crossing points' of the patterns could be problematic with this type of deformation.

5.4 Sclera Matching Results

5.4.1 Example Individual Matching Result

An example matching result is shown as Figure 5.2. This shows two vein templates (in blue and red), and matching results in green. Note that one of the templates is artificially and intentionally shifted to allow the matching results to be more easily seen. Additionally, the author acknowledges that this image is somewhat difficult to see, due to the small size of the individual segments, but it is retained to show that the entire sclera region is matched. Further examples will show more readable examples showing particular sections of the matching.

Figure 5.3 shows the original images used in Figure 5.4, and the segmented and enhanced vein patterns (before thresholding or morphological operations). The images (a) and (b) are from the same user, and image (c) is from a different user.

Figure 5.4 shows two zoomed in matching results — the top matching result is for two separate images from the same user (which should match), and the bottom shows matching results from two separate images of two separate users (which should not match). In each of the examples in Figure 5.4, the first user's first image (in red in the images) is matched to 2 other images (in blue in the images) — one of which it should match to (from the same user), and one that it should not (from a different user). The images in the middle of the figure are blown up for ease of viewing. The images show the two vein patterns, and the green lines indicate where matches were found. The color of the green lines indicates the strength of the match, a more bright tone is a stronger or more confident match, and duller tones indicate less strong matches. As the matching results on the right of the image show, the matching results correspond with the ground truth of the particular matching results.

Figure 5.2 Example matching results. The test vein patterns are in red, the target patterns are blue, and the short green lines indicate matches between two segments.

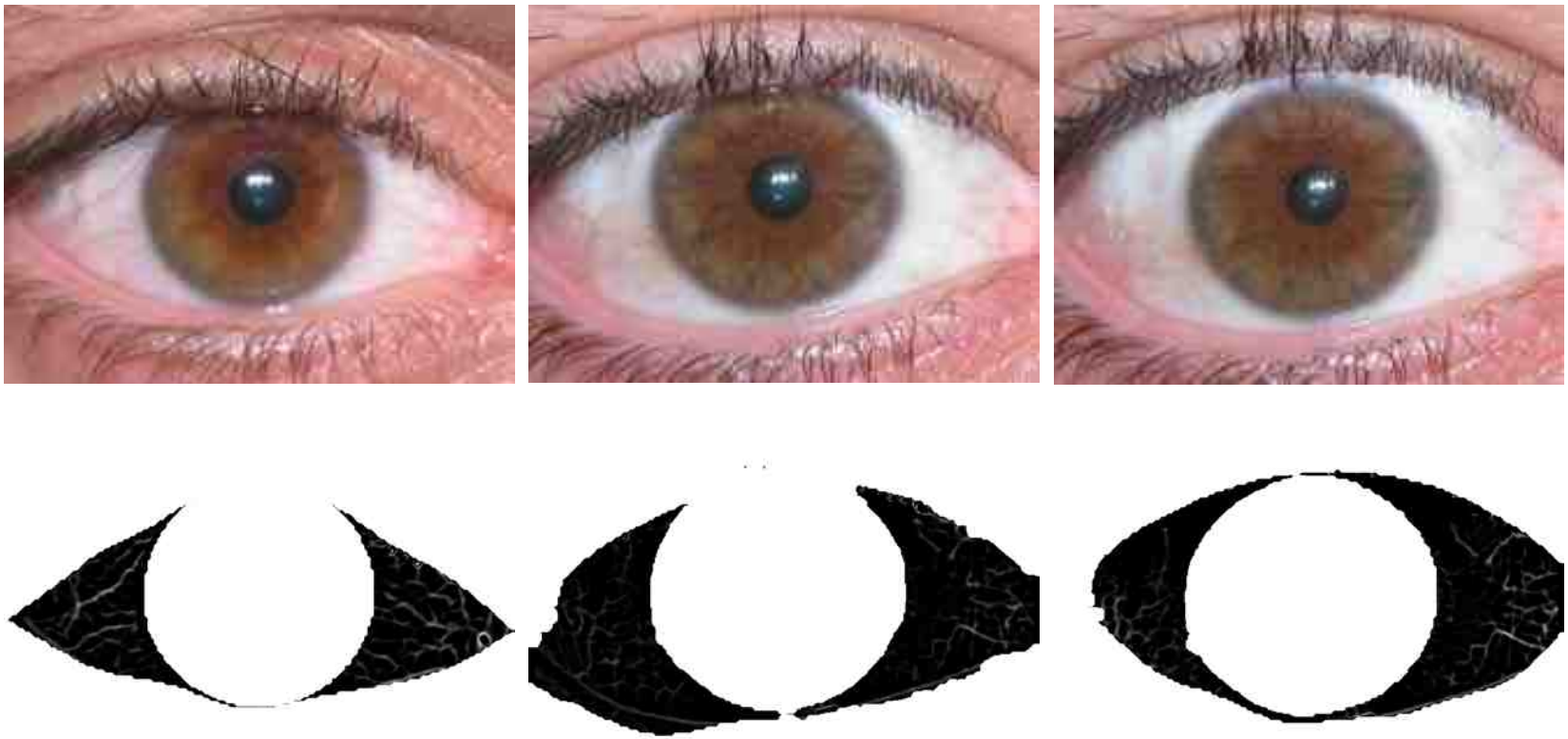

(a) (b) (c)

Figure 5.3 The original images, and the Gabor enhanced images used for the matching example in Figure 5.4. The Gabor enhanced images are paired with the original images above them. From left to right: (a) user 1, image 1; (b) user 1, image 4; (c) user 2, image 1

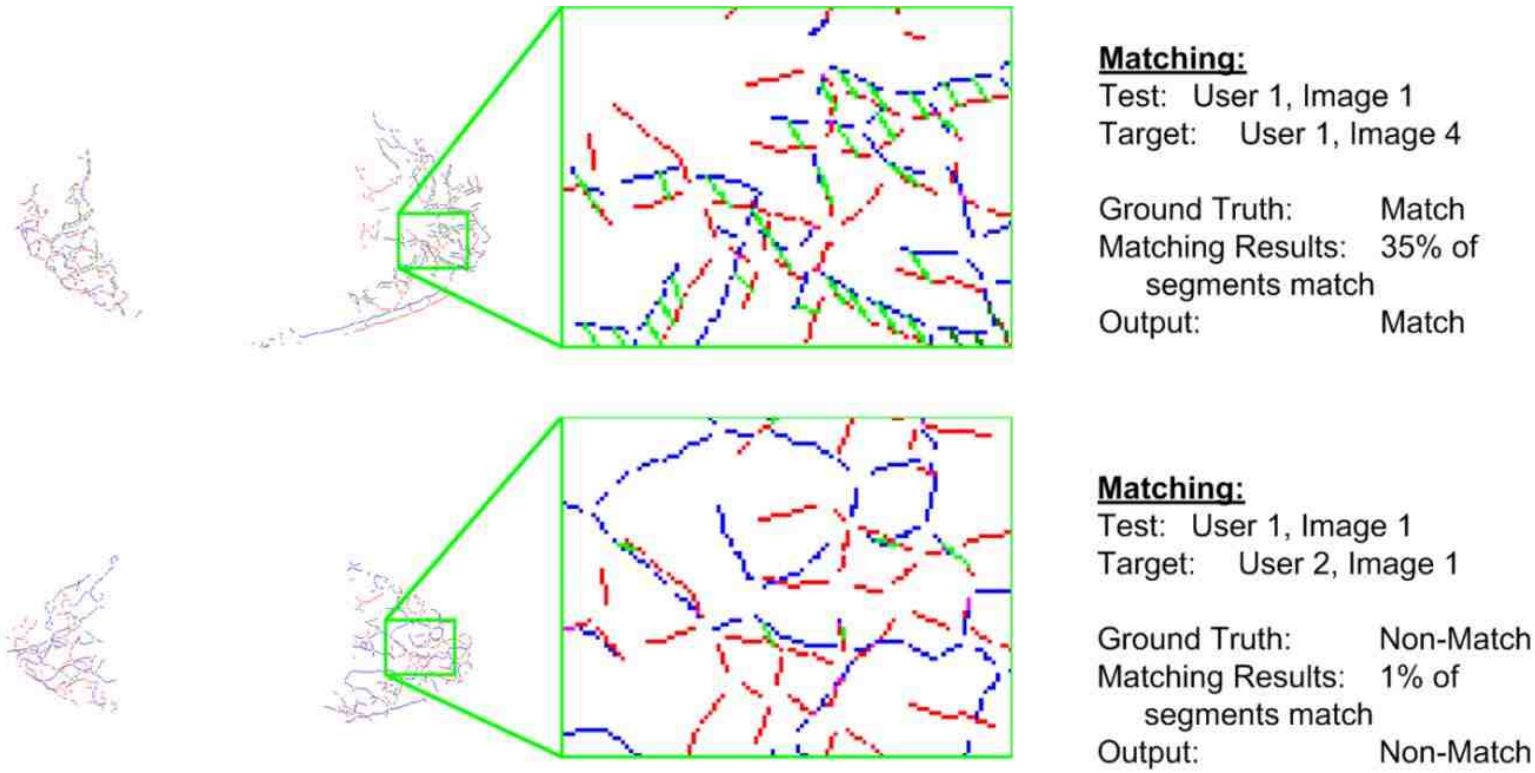

Figure 5.4 Example matching results. (a) The sclera patterns are well matched from 2 images of the same person. (b) The sclera patterns are not matched from 2 images of different persons. The red and blue patterns are the test and target users patterns, and the green lines indicate matches found.

5.4.2 UBIRIS Database Matching Results

The overall matching results were computed for an all-to-all similarity matrix. For this work, the first session of the UBIRIS database was used, which includes 1214 images from 241 users. The second session of the database was excluded because those images were not acquired with sufficient quality to extract the sclera vein patterns. Using the 1205 images (99.26% of the database) that were able to be segmented in the UBIRIS, session 1, database there are over 1.4 million cross-comparisons with an equal error rate of 3.38% and an ROC error area of 2.04%. The distribution of genuine and imposter matching scores for the UBIRIS-session 1 database is shown in Figure 5.6(a). Note that the genuine and imposter distributions are well separated in general, with the exception of a spike in the genuine and imposter distribution at a matching value of 1. This is due to the matching algorithm assigning a matching value of 1 to those matches with less than 20 matching segments, but with a matching percentage greater than 5%. This keeps poor quality images with very small extracted vein patterns from having arbitrarily high matching results.

Very poor quality images, such as those in the third row of Figure 1.3, tend to have very few extracted vein patterns. These images are removed from the 'image quality control' matching results, by using a threshold T to remove images with a number of matching segments less than T. For the UBIRIS database (session 1), sixty six (66) of 1205 images are removed (5.48% of the total number of images) due to very poor quality An example of a specific image that is of such poor quality to be unrecognizable, due to very few extracted veins and poor image quality, is shown in Figure 5.5.

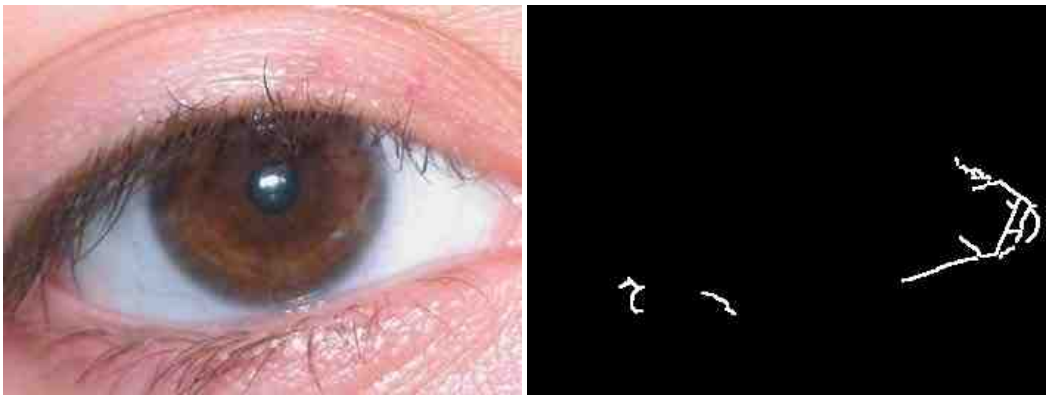

Figure 5.5 An example image of a poor quality image with few extracted veins. Note that the vein structure was morphologically dilated for ease of viewing.

With the image quality control (by excluding those images with a number of matches less than T), the calculated equal error rate is reduced to 1.03% and the ROC error area to 0.14%. Figure 5.6(b) shows the genuine and imposter distributions after image quality control. The ROC curves for both the entire database and after image quality control is shown in Figure 5.7.

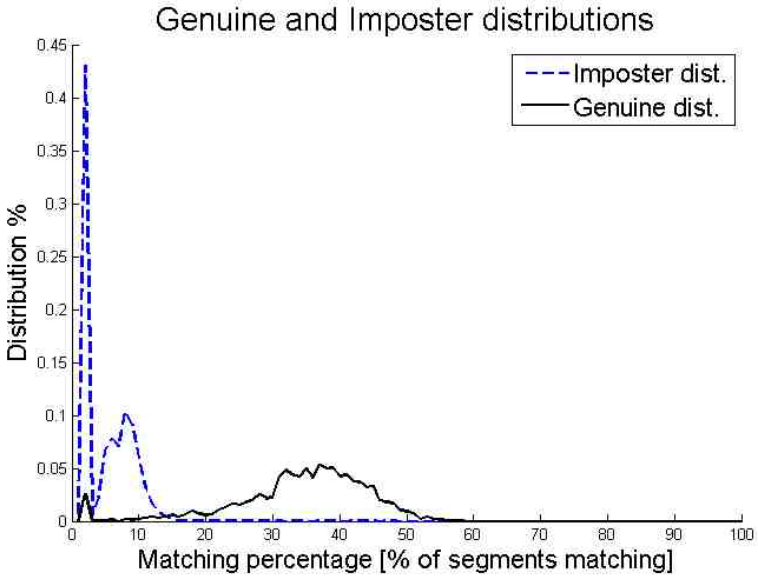

(a)

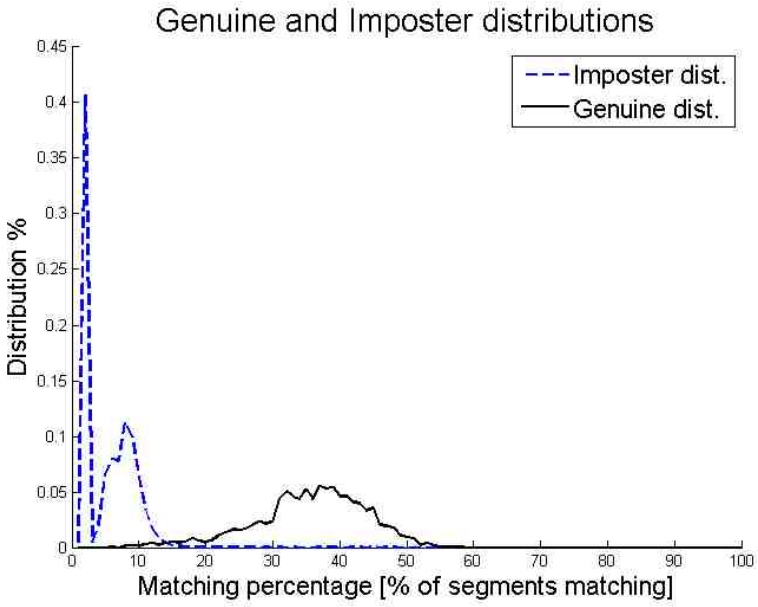

(b)

Figure 5.6 (a) The distribution of matching scores for the entire database. (b) The distribution of matching scores for the database, after image quality control.

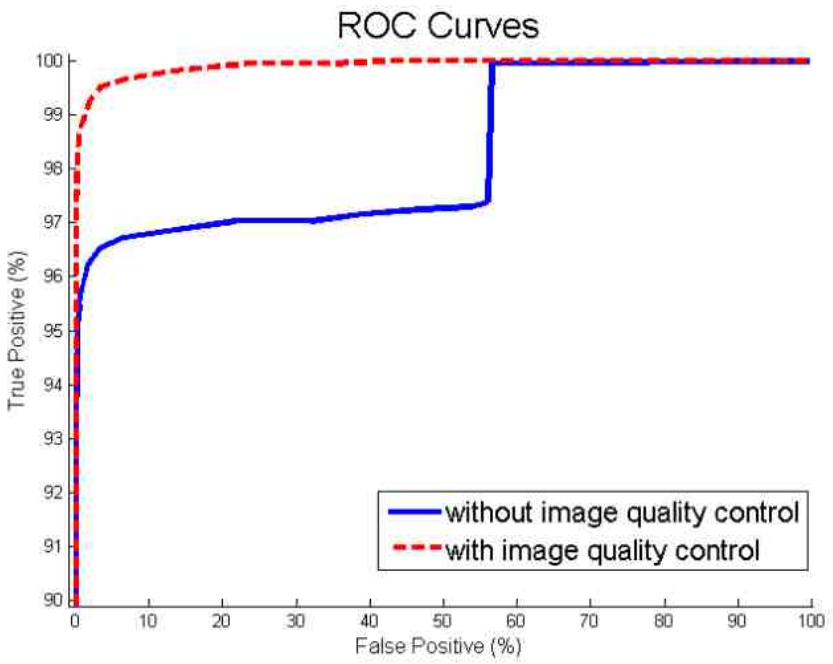

Figure 5.7 The ROC curves for the system. Note that the y-axis is scaled from 90-100% for ease of viewing.

Finally, we give matching results for the entire UBIRIS database. In this case, 1732 images were able to be segmented and matched (92.2%), with a calculated EER of 20.71% and an ROC error area of 16.64%. Figure 5.8 shows the distribution of matching scores for the entire UBIRIS database, and Figure 5.9 shows the ROC curve for the entire UBIRIS database. These results have much lower accuracy than the previously reported results and it is primarily due to the fact that the UBIRIS database, session 2, is of very poor quality (Figure 1.4 and Figure 1.5). The second session was specifically intended to simulate very poor quality non-compliant image acquisition, and as such, has very poor focus, large saturation regions, and other noise. As mentioned earlier, the UBIRIS database was not originally intended to be used for sclera recognition, so much of the data, especially the session 2 data, is not of adequate quality for high-confidence sclera recognition. However, noting these issues, the imposter distribution in Figure 5.8 is still well clustered, which implies that with better quality data, and perhaps better registration, the proposed system could perform with similar accuracy as in the other reported results.

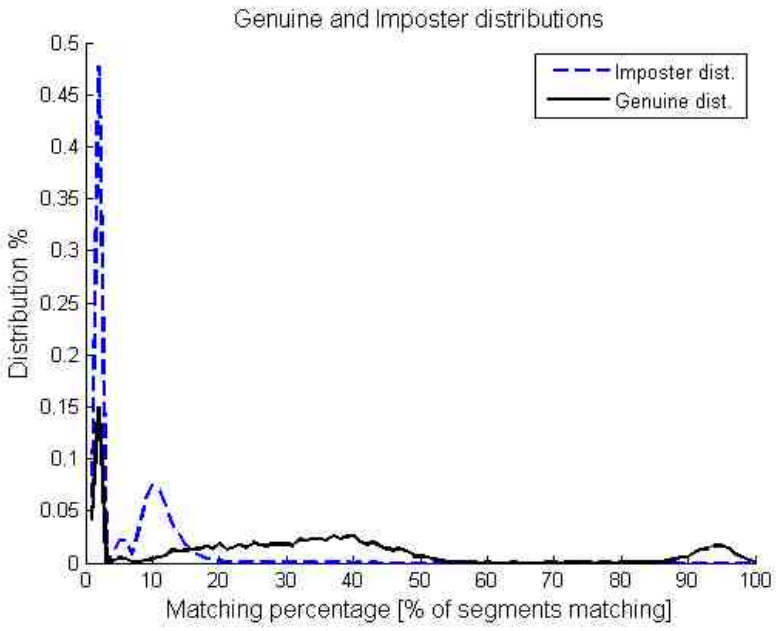

Figure 5.8 The distribution of matching scores for the entire UBIRIS database

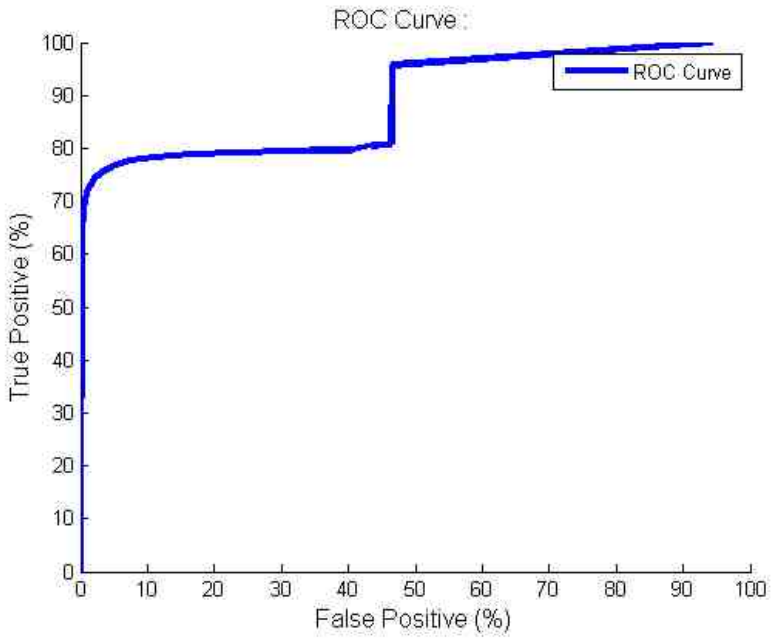

Figure 5.9 The ROC curve for the entire UBIRIS database

The EER and ROC error area of matching the UBIRIS images from session 1 to session 2 are 36.64% and 27.29%, respectively. Figure 5.10 shows that the imposter distribution remains well-clustered as in previous experiments. However, the average matching score for genuine matches is significantly lower (~20%, excluding the peak at 1%). Figure 5.11 shows the ROC curve for matching session 1 to session 2 of the UBIRIS database. The EER and ROC error area of matching session 2 to session 2 of the UBIRIS database are 17.53% and 23.60%, respectively. Figure 5.12 shows the distributions of matching scores when matching session 2 to session 2, and Figure 5.13 shows the ROC curve. When comparing session 2 to session 2, we can see that the average genuine matching score (of the lower cluster in the genuine distribution) is almost 20 points higher (from ~40% in Figure 5.12 to ~20% in Figure 5.10) as compared to matching across the sessions.

These results demonstrate that the UBIRIS database, session 2, is of very poor quality for sclera recognition. This is not surprising, as the database was not acquired with the intention of being used for sclera recognition. Note, however, that one can see that the imposter distribution is very similar even when matching across the sessions. This means that, even if the matching results are low, the system will not have an arbitrarily high false accept rate, as none of the experiments have any significant imposter scores above a threshold of around 20%.

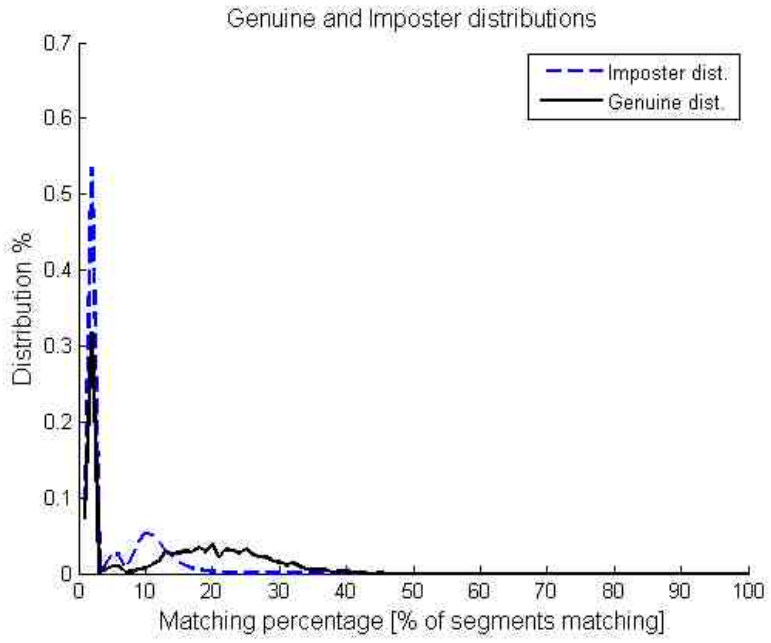

Figure 5.10 The distribution of matching scores for session 1 matched to session 2 of the UBIRIS database

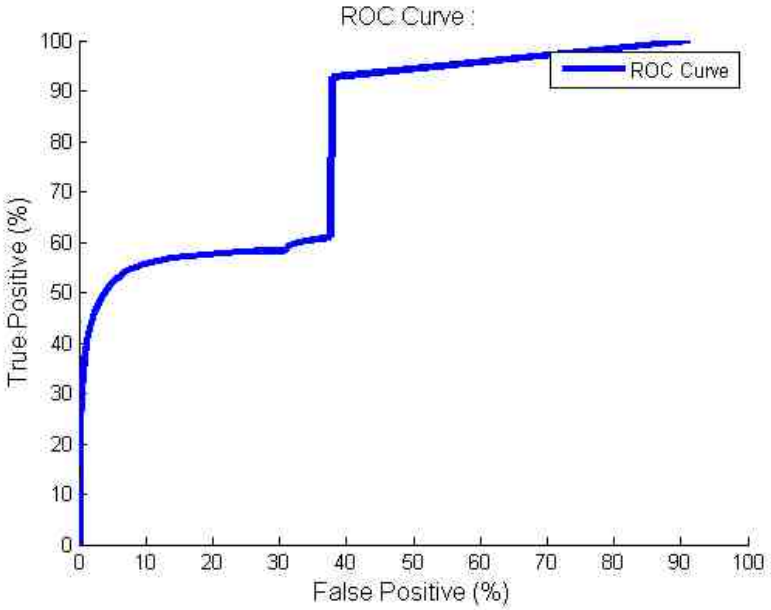

Figure 5.11 The ROC curve for session 1 matched to session 2 of the UBIRIS database

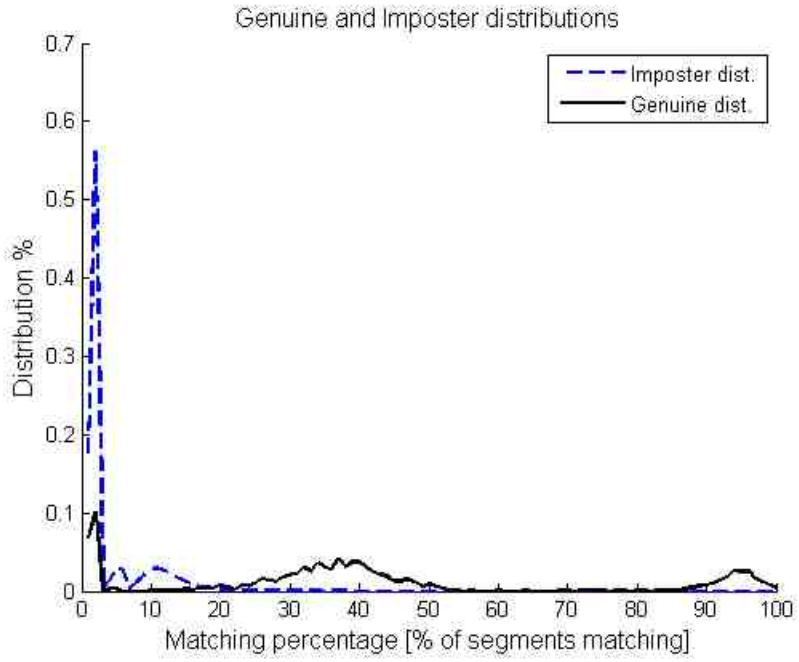

Figure 5.12 The distribution of matching scores for session 2 matched to session 2 of the UBIRIS database

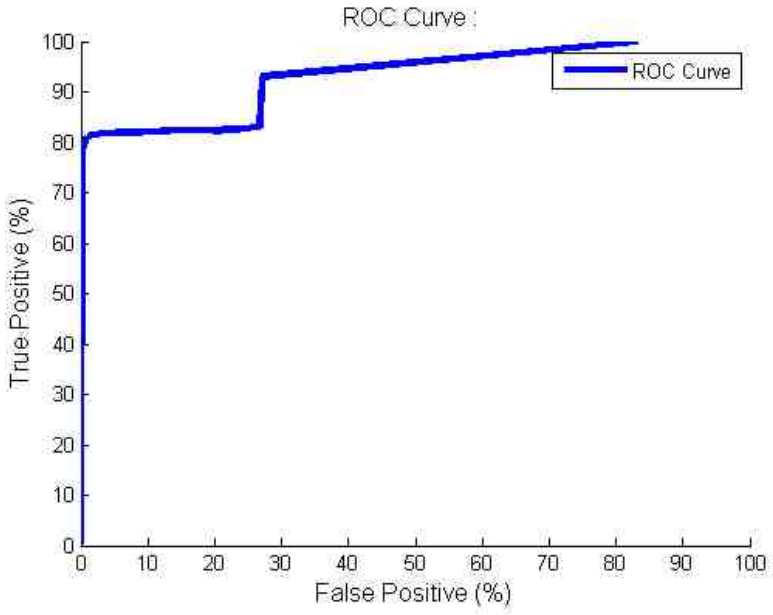

Figure 5.13 The ROC curve for session 2 matched to session 2 of the UBIRIS database

5.4.3 Matching Results for IUPUI Multiple Wavelength Database

For the IUPUI multi-wavelength database, results are presented for the left eyes. For the left eyes, an all-to-all comparison of the left eyes of the users was calculated, with a total of 178 images. Two frontal-gaze images were manually selected from the 525nm videos for each user, and manual segmentation was used to segment the sclera region.

For the left eye case, there was a calculated EER of 4.78%, with an ROC error area of 2.49%. Figure 5.14 shows the distribution of matching scores for the left eye case, and Figure 5.15 shows the ROC curve. These results are somewhat lower than for the UBIRIS database, which seems counter-intuitive given that the images were manually selected and segmented. However, due to the more significant noise and focus problems inherent in the non-compliant nature of the IUPUI multi-wavelength database, the overall quality of the images is less consistent than in the UBIRIS database, which could account for the somewhat less accurate results. Additionally, since the total number of images used is much smaller, a few poor quality images have a stronger influence in the overall matching results, as compared to the much larger UBIRIS database.

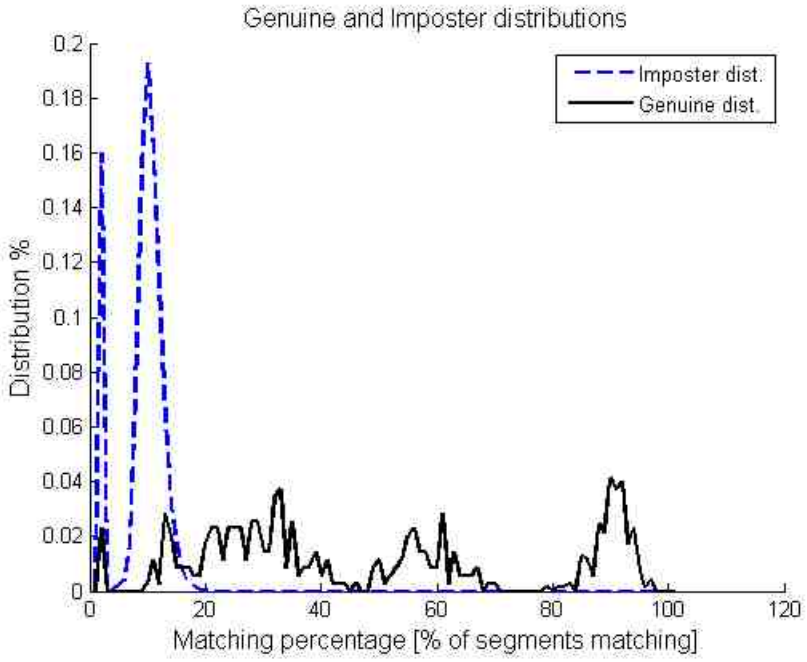

Figure 5.14 The distribution of matching scores for the IUPUI multi-wavelength database, left eyes only

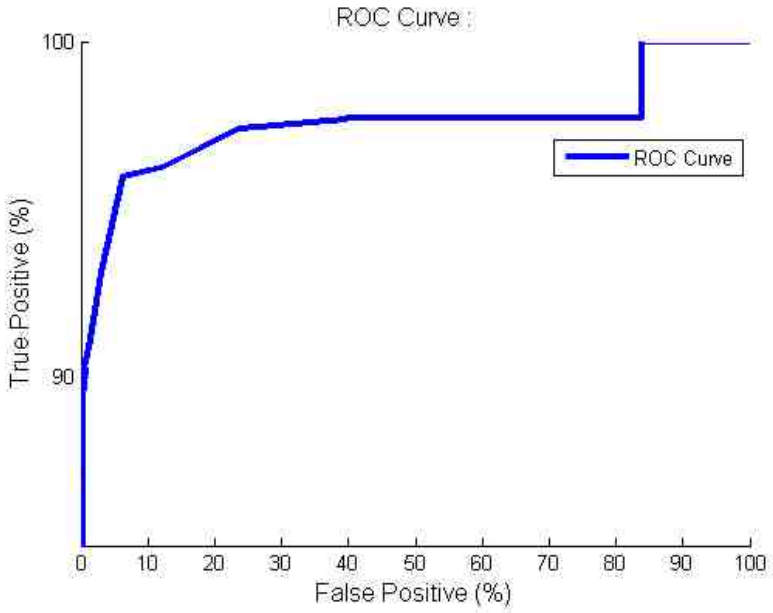

Figure 5.15 The ROC curve for the IUPUI multi-wavelength database, left eyes only. Note that the y-axis is scaled from 85-100% for ease of viewing.

5.4.4 Challenging Cases for Sclera Matching

For sclera matching, there were three major cases that caused matching difficulty.

- Images with incorrectly extracted vein patterns
- Images with very small sclera regions, and similarly few detected veins
- Images that were not properly registered

For the first two problems, the issues create difficulties in properly matching all extracted veins in the sclera region, and for the last, it creates problems in properly matching sclera patterns.

First, for any images, like those discussed in Section 4.4.1, where the vein pattern was not able to be reliably extracted due to poor image quality, the matching results may not be consistent due to the inconsistency of the extracted vein patterns.

In the following images, we present an example of an image with a very small sclera region, and a particular matching case where it resulted in an artificially high matching score for a matching scenario that should not have matched. First, in Figure 5.16 we show the original test image, in Figure 5.17 we show the target image, and in Figure 5.18 we show the matching results. Note that in the matching results, the percentage of matching segments is arbitrarily high because of the small sclera region, and therefore the small number of extracted and possible segments.

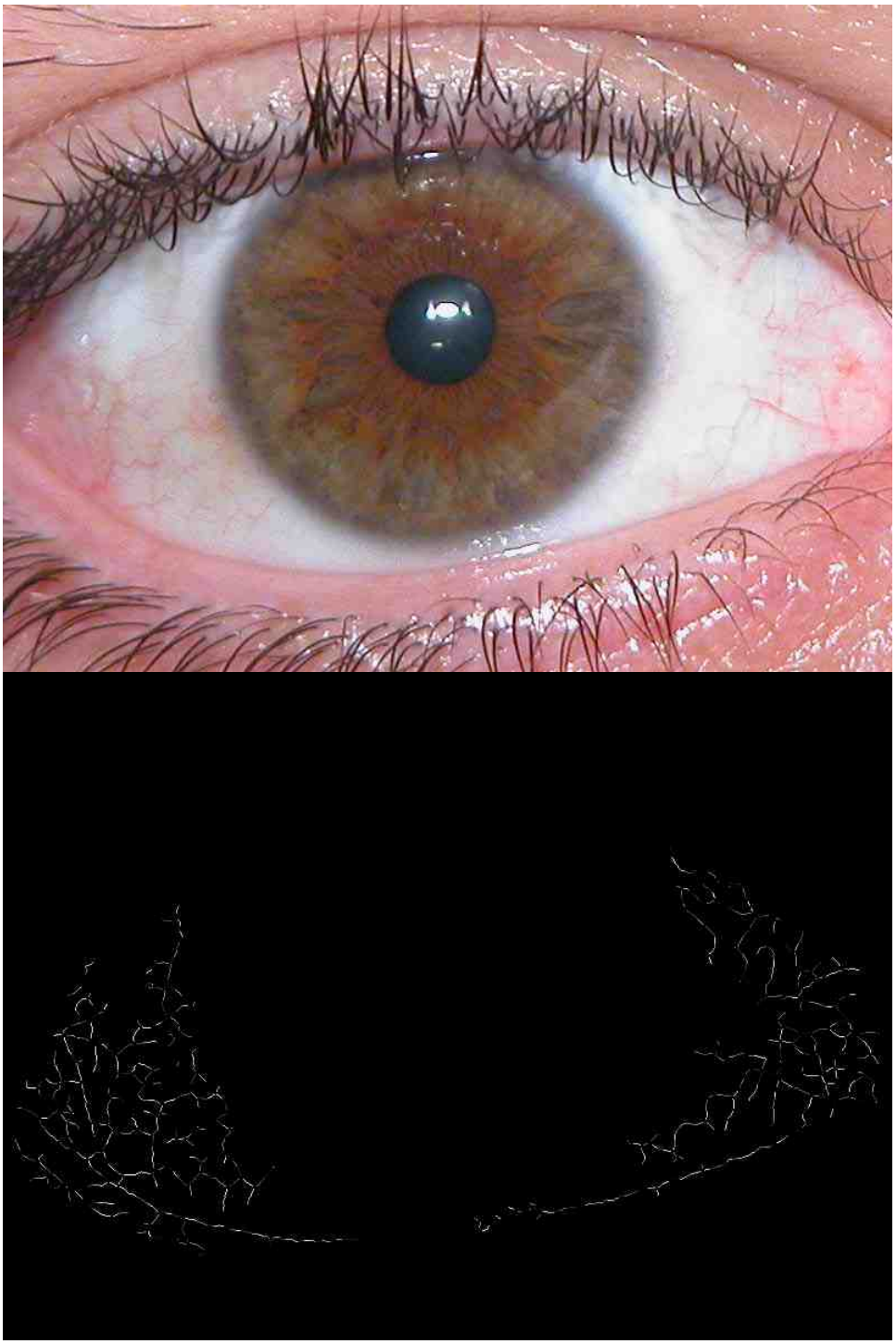

Figure 5.16 The test image and the detected sclera veins for the small sclera region case

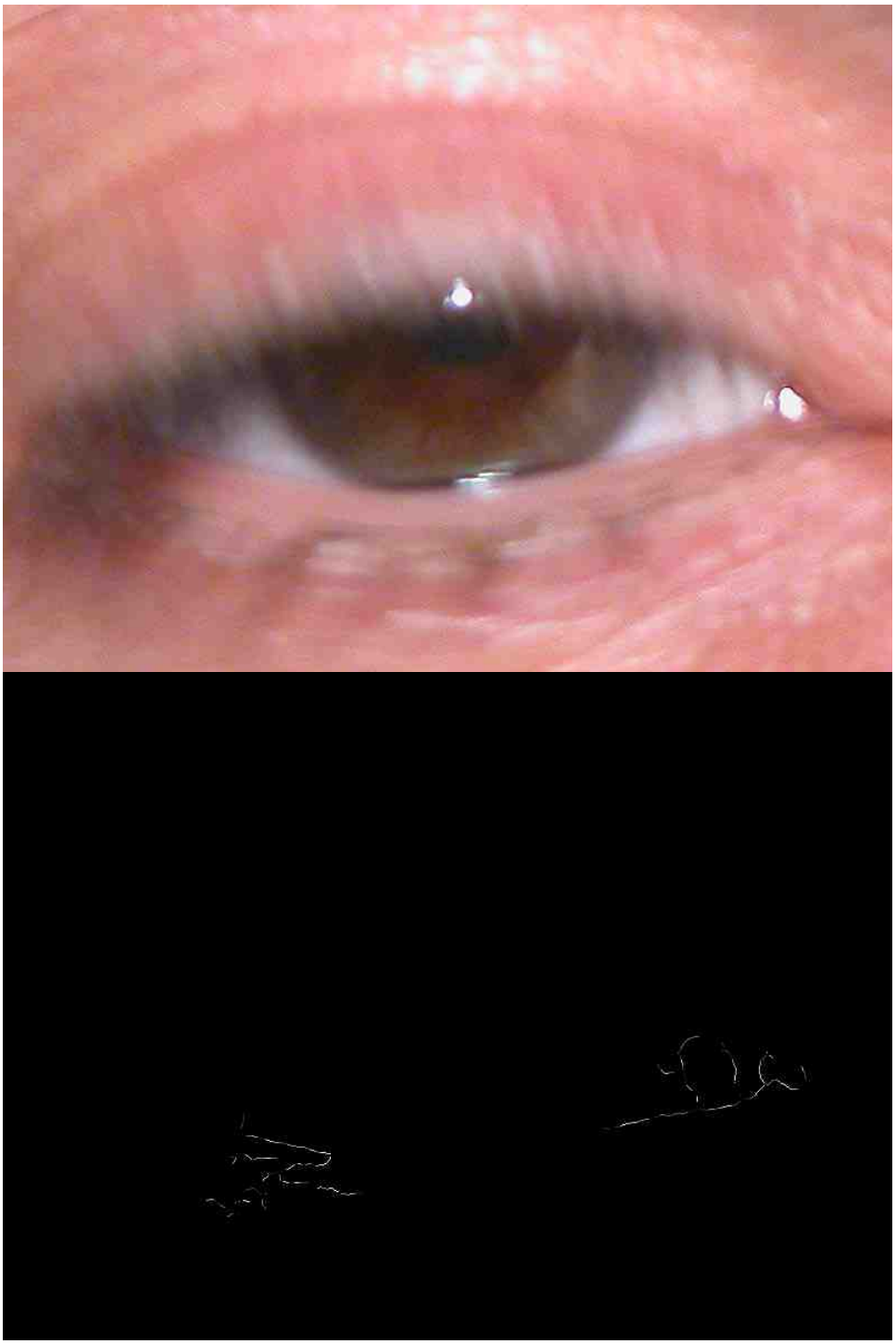

Figure 5.17 The target image and the detected sclera veins for the small sclera case

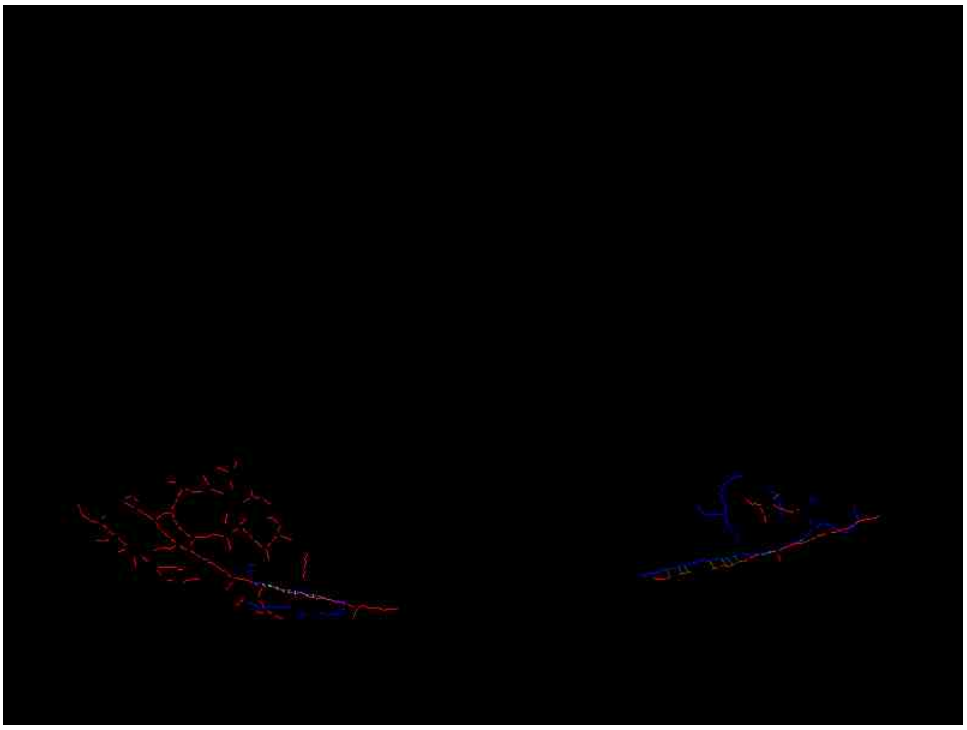

Figure 5.18 The matching result for the small sclera case

Lastly, in the following figures we present an example of a pair of images that should match, but were not properly registered. As a result, the images had a low matching score that indicated that they should not match, when, in fact, their ground truth was that they should match. In Figure 5.19 we show the test image, in Figure 5.20 we show the target image, and in Figure 5.21 we show the matching results. In this particular case, these two images are from the same user, and therefore, should match. Due to the mis-registration of the two sclera patterns, the matching score was 7%, significantly under a typical matching threshold of 16%, for the UBIRIS database. In this case, the proper registration would have required that the blue descriptor be moved up to correspond better with the red pattern. Most likely, these two patterns' detected iris centers were significantly different, and as such the proper registration was outside of the search range for the registration algorithm.

Figure 5.19 The test image from the mis-registration example

Figure 5.20 The target image from the mis-registration example

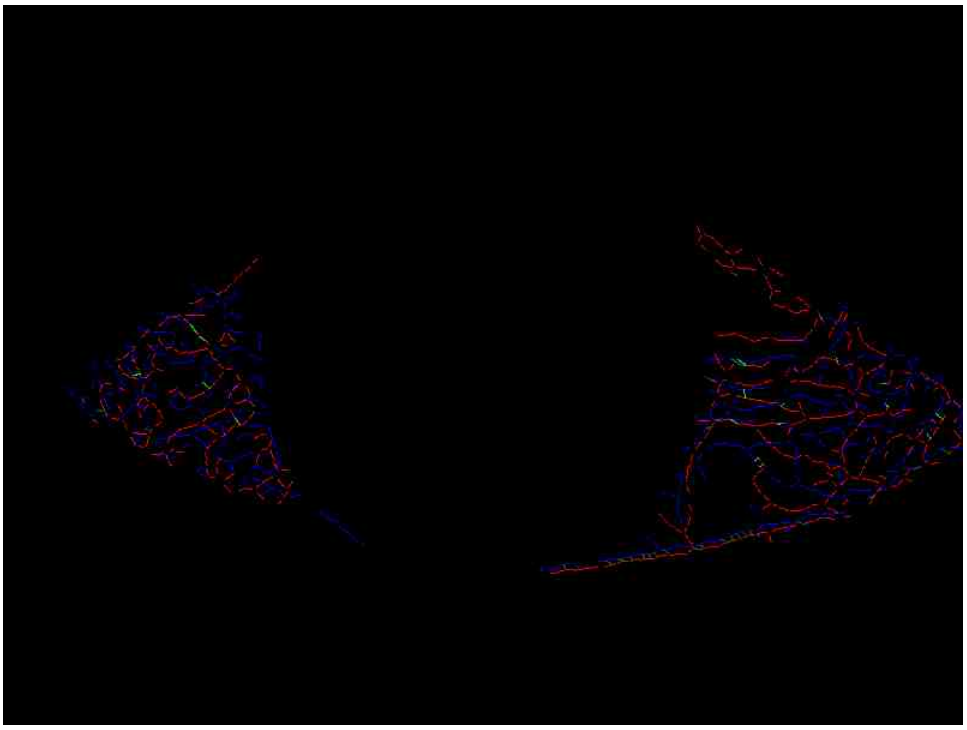

Figure 5.21 The matching results from the mis-registration example

5.5 Summary

In this section, sclera vein descriptor registration and matching algorithms are presented. The registration algorithm is a RANSAC-type algorithm that searches for the optimum set of registration parameters that minimizes the summed pairwise distance between the two templates to be registered. This is the first sclera registration system to be presented or proposed that can robustly register the sclera vein patterns even with their inherent multi-layered, non-linear deformation. A matching algorithm is proposed that allows for matching in the presence of the same deformation. Overall, a comprehensive system is presented for matching sclera vein patterns acquired under non-compliant situations.

Results for both the UBIRIS and IUPUI multi-wavelength databases are presented. The distribution of matching scores for both databases experimentally

demonstrates that the sclera vein pattern is appropriate for use as a biometric identifier – i.e., the matching distributions for imposter and genuine matches are significantly separable. Equal error rates were calculated to be 3.38% for the UBIRIS database, session 1, and 4.78% for the IUPUI multi-wavelength database, using left eyes at 525nm illumination. These results are significantly more accurate than previously reported results for sclera recognition — for example, 3.38% EER for the proposed system with automatic segmentation and a large database compared to ~25% EER with semi-automated segmentation and a much smaller database. This is the first work that presents the results for sclera recognition using a publicly available database to allow for repetition and direct comparison to other methods. The results, for the largest experiment, presented represent over 1.4 million cross-comparisons of sclera images which is significantly larger than the largest previous experiment, which included under twenty-three thousand total cross-comparisons.

These results show a significant improvement over the existing state-of-the-art sclera recognition matching algorithms, and could make sclera recognition a viable alternative for non-compliant recognition applications.

6. COMPARISON TO IRIS RECOGNITION IN VISIBLE WAVELENGTHS

6.1 Comparison of Results

6.1.1 Comparison with UBIRIS Database

To give a performance reference for these matching results as compared to other biometric modalities using the same database, we compare our results using the proposed sclera recognition system to those reported by Proenca and Alexandre in [55] for visible wavelength iris recognition. For their system, the selected 800 images from the UBIRIS database (42.6% of the entire database), however, they do not report how they selected the 800 images. They partition the iris into 6 separate regions, encode the individual regions using Daugman's method as outlined in [4], and utilize a score fusion scheme to minimize the effect of noise (due to the non-compliant nature of the data). Table 6.1 compares equal error rates (EER) and the receiver operating curve (ROC) error area for two of their reported methods and the proposed method, to show the validity of sclera vein recognition in relation to a more established biometric modality, iris recognition. Note, however, that both of these results suppose poor quality data (such as would be expected in a non-compliant or surveillance biometric system), an operational environment that Daugman's algorithms were not originally intended or designed to be used. As such, these results are not intended to propose that sclera recognition could provide similar results to iris recognition using high quality, near-infrared acquired, and compliant iris/eye images. Table 6.2 shows the False Rejection Rates (FRR) for the proposed system at different set False Acceptance Rates (FAR).

Table 6.1 Comparison of EER's for different matching modalities and methods on the UBIRIS database

Modality	Method	# of Images Used	EER (%)	ROC Error (%)
Iris	Proenca and Alexandre [55]	800	2.38	1.73
Iris	Daugman [55]	800	3.72	3.21
Sclera	Proposed – without image quality control	1205	3.38	2.04
Sclera	Proposed – with image quality control	1139	1.03	0.14

Table 6.2 FRR for given FAR's for the proposed method

Modality	Method	# Images Used	FRR (%), FAR=1.0%	FRR (%), FAR=0.1%	FRR (%), FAR=0.01%
Sclera	Proposed – without image quality control	1205	4.21	5.89	9.53
Sclera	Proposed – with image quality control	1139	1.14	2.72	5.15

This shows that for low quality, visible light images, sclera recognition can be used with comparable matching results to iris recognition technologies. Additionally, it could be used in conjunction with iris recognition, face recognition, or other facial biometric modalities to provide higher accuracy and confidence in the matching results.

6.1.2 Comparison with IUPUI Multiple Wavelength Database

For the IUPUI multi-wavelength database, results were computed using both Daugman's 2-D Gabor [6] and Masek's Log-Gabor [72] iris recognition systems that were programmed in-house using Matlab. All images were hand selected, and hand segmented. The results for the left eyes with wavelength three (525nm) illumination from this database is presented in Table 6.3.

Table 6.3 Comparison of proposed method versus iris recognition methods for wavelength 3 of the IUPUI multi-wavelength database

Method	**# Images Used**	**EER**	**FRR (%), FAR=1.0%**	**FRR (%), FAR=0.1%**	**FRR (%), FAR=0.01%**
Iris - Gabor(LogPolar)	178	8.49	22.83	38.30	50.38
Iris - LogPolar(LogGabor)	178	13.64	28.11	35.47	47.74
Sclera - Proposed	178	4.78	9.71	11.43	12.00

6.2 Summary

To give a comparison of the proposed system to more established biometric modalities, the proposed systems results on two databases are compared to iris recognition on those same databases. First, the proposed system is compared to state-of-the-art visible wavelength iris recognition results using the UBIRIS database, with very comparable results. Second, the proposed system's results are compared to benchmark iris recognition algorithms, Daugman's 2-D Gabor and Masek's log-Gabor algorithms, using one wavelength of the IUPUI multi-wavelength database. In comparison to these benchmark iris recognition algorithms, the proposed sclera recognition algorithm was significantly more accurate.

7. CONCLUSION

In this work, a completely automated system was developed that can accurately identify individuals using their sclera vasculature patterns, with potential implementations as either a uni-modal configuration or as a multi-modal configuration with another biometric modality. The system can use visible light acquired images — which can be acquired at longer distances and in more varied operational environments than traditional iris recognition systems. The system uses a biometric modality, the sclera vasculature, which is well-suited to non-compliant situations — it is easily imaged in the visible frequencies, is difficult to hide or disguise, is difficult to forge, and is highly unique.

This type of visible light acquired biometric system has the potential to expand the operational range of biometric systems in surveillance and non-compliant situations. These types of implementations could significantly increase the ability to maintain public security while being unobtrusive and user-friendly.

A new color-based sclera segmentation system was developed that uses a color-based sclera estimation scheme along with an active contour refinement to segment the sclera region. In addition to being used for sclera recognition, the sclera segmentation system could also be used as an intermediary step in color iris segmentation, similar to [53], for use in non-compliant iris recognition systems. Currently, to the authors knowledge, this is the only system that can accurately segment the sclera region without manual intervention or training.

A Gabor filter based vein enhancement and extraction system was developed, along with a novel line descriptor method for vein template generation. This system can robustly enhance the vein structure, and can describe the multi-layered structure of the veins in a way that can be identified, even with the complex, layered, non-linear deformation that the vein structure undergoes.

A matching scheme was developed to register and match the developed line descriptors. The registration algorithm can register the line descriptors without over-fitting (thus limiting the false acceptance rate), while still accommodating the aforementioned sclera vein pattern deformations. Additionally, when compared to the existing state-of-the-art implementations of iris recognition algorithms in the visible frequencies, the proposed system performed with similar results (3.38% EER for the proposed system vs. 2.38% for iris recognition).

Finally, in comparison to the previous sclera recognition algorithms, the proposed method has been tested and verified on a much larger scale — for example, the UBIRIS database's all-to-all comparison results include more than 64 times the total number of individual comparisons of the largest similar previous work (~1.4 million to ~23 thousand). The proposed system is entirely automated, where all previous works were either entirely manual or included very significant manual components or intervention. While an exact comparison cannot be provided due to the internal databases used in previous works, in comparison to the most recent and most comparable results presented in [28] (i.e., the largest database with the least manual intervention), the proposed system had an EER of 3.38% without image quality control as compared to the previous algorithms reported results of ~25% EER.

Both the UBIRIS database and the IUPUI multi-wavelength databases were used to provide experimental results, which show that the proposed sclera recognition method can achieve better results than previous sclera recognition algorithms and comparable recognition accuracy to state-of-the-art iris recognition algorithms, with the same visible-

light, low-quality images. This shows that sclera vein recognition is very promising to be used as a primary biometric method in the near future for non-compliant or surveillance biometric identification or in parallel with existing primary biometric modalities, namely iris and face recognition.

To the best of the author's knowledge, this is the first system fully automated sclera recognition system. Lastly, the presented results incorporate much larger experiments than previous works, and are the first to provide results for sclera recognition using a publicly available database.

7.1 Future Works

The sclera segmentation algorithm could be refined. The accuracy of the segmentation results could be better, especially around the lower eyelid boundary near the tear ducts. Additionally, it may be useful to have a segmentation algorithm that was equally capable on either color or grayscale images to allow for broader implementation in existing biometric and surveillance systems.

The registration algorithm could be improved by incorporating a 3-D model of the eye. Especially when using unconstrained eye images, it is important to have a robust and efficient registration algorithm that can account for the 3-dimensional nature of the eye. Currently, the author believes that a possible obstacle to lower EER's is performing more consistent registration of sclera vein templates when acquired at different times, with different postures, stand-off distances, etc.

Algorithms that can create a 'whole eye' template from multiple images, or video, of the eye at different gaze angles could be developed, and the appropriate changes to the registration algorithms to allow matching using them. The goal of this type of biometric modality is to provide non-compliant and unconstrained matching, and to allow this, it

might be useful for the system to be able to match an individual with little or no constraints on the gaze angle of the eye.

An algorithm that is able to estimate, and match, the individual constituent veins from the template could be developed. The author believes that the algorithms accuracy might be improved if the matching algorithms registered and matched each of the constituent veins in the template individually. Additionally, this may allow the deformation of individual vein structures to be used as a biometric identifier for liveness tests, fraud detection/prevention, and identification. Care must be taken to ensure that this type of registration/matching does not over-fit the identifier, as both the false-acceptance rate and the false-rejection rate are important in practical systems.

Lastly, before any practical deployment of the proposed system, the proposed algorithms could be tested on a larger scale – using millions of sclera images, for instance. The scale that would be useful for pre-deployment tests is not practical, either from a time or cost standpoint, for an academic work, but it could be useful to debug any issues that may exhibit themselves when the proposed system is implemented on a larger scale.

LIST OF REFERENCES

LIST OF REFERENCES

[1] J. Daugman, "Probing the Uniqueness and Randomness of IrisCodes: Results From 200 Billion Iris Pair Comparisons," *Proceedings of the IEEE,* vol. 94, pp. 1927-1935, 2006.

[2] "US $10 million order for SecuriMetrics," *Biometric Technology Today,* vol. 14, pp. 4-4, 2006.

[3] M. A. Sasse, "Red-Eye Blink, Bendy Shuffle, and the Yuck Factor: A User Experience of Biometric Airport Systems," *IEEE Security & Privacy,* vol. 5, pp. 78-81, 2007.

[4] J. Daugman, "High confidence visual recognition of persons by a test of statistical independence," *IEEE Transactions on Pattern Analysis and Machine Intelligence,* vol. 15, pp. 1148-1161, 1993.

[5] J. Daugman, "Demodulation By Complex-Valued Wavelets For Stochastic Pattern Recognition," *International Journal of Wavelets, Multi-resolution and Information Processing,* vol. 1, pp. 1-17, 2003.

[6] J. Daugman, "How iris recognition works," *IEEE Transactions on Circuits and Systems for Video Technology,* vol. 14, pp. 21-30, 2004.

[7] J. Daugman, "New Methods in Iris Recognition," *IEEE Transactions on Systems, Man, and Cybernetics, Part B,* vol. 37, pp. 1167-1175, 2007.

[8] J. R. Matey, O. Naroditsky, K. Hanna, R. Kolczynski, D. J. LoIacono, S. Mangru, M. Tinker, T. M. Zappia, and W. Y. Zhao, "Iris on the Move: Acquisition of Images for Iris Recognition in Less Constrained Environments," *Proceedings of the IEEE,* vol. 94, pp. 1936-1947, 2006.

[9] NIST, "NIST ICE Iris Image Database," 2007.

[10] Y. Du, N. L. Thomas, and E. Arslanturk, "Multi-level iris video image thresholding," in *IEEE Workshop on Computational Intelligence in Biometrics: Theory, Algorithms, and Applications*, 2009, pp. 38-45.

[11] Y. Du and E. Arslanturk, "Video based non-cooperative iris segmentation," in *Proceedings of SPIE*, 2008.

[12] C. Belcher and Y. Du, "A Selective Feature Information Approach for Iris Image-Quality Measure," *IEEE Transactions on Information Forensics and Security*, vol. 3, pp. 572-577, 2008.

[13] Z. Zhou, Y. Du, and C. Belcher, "Transforming Traditional Iris Recognition Systems to Work in Nonideal Situations," *IEEE Transactions on Industrial Electronics*, vol. 56, pp. 3203-3213, 2009.

[14] C. Belcher and Y. Du, "Region-based SIFT approach to iris recognition," *Optics and Lasers in Engineering*, vol. 47, pp. 139-147, 2009.

[15] C. Belcher and Y.Du, "A New Approach for Non-Cooperative Iris Recognition," *SPIE Defense and Security*, vol. 7351, 2009.

[16] H. Proença and L. A. Alexandre, "UBIRIS: A noisy iris image database," *13th International Conference on Image Analysis and Processing*, vol. Springer LNCS 3617, pp. 970-977, 2005.

[17] C. Boyce, A. Ross, M. Monaco, L. Hornak, and L. Xin, "Multispectral Iris Analysis: A Preliminary Study," in *Conference on Computer Vision and Pattern Recognition Workshop*, 2006.

[18] A. Ross, R. Pasula, and L. Hornak, "Exploring multispectral iris recognition beyond 900nm," in *IEEE 3rd International Conference on Biometrics: Theory, Applications, and Systems*, 2009, pp. 1-8.

[19] N. A. Rahman, A. S. Mohamed, and M. E. Rasmy, "Retinal Identification," in *Cairo International Biomedical Engineering Conference*, 2008, pp. 1-4.

[20] H. Borgen, P. Bours, and S. D. Wolthusen, "Visible-Spectrum Biometric Retina Recognition," in *Proceedings of the International Conference on Intelligent Information Hiding and Multimedia Signal Processing*: IEEE Computer Society, 2008.

[21] M. E. Martinez-Perez, A. D. Hughes, A. V. Stanton, S. A. Thom, A. A. Bharath, and K. H. Parker, "Segmentation of retinal blood vessels based on the second directional derivative and region growing," in *Proceedings of International Conference on Image Processing*, 1999, pp. 173-176. vol. 2.

[22] H. Narasimha-Iyer, J. M. Beach, B. Khoobehi, and B. Roysam, "Automatic Identification of Retinal Arteries and Veins From Dual-Wavelength Images Using Structural and Functional Features," *IEEE Transactions on Biomedical Engineering,* vol. 54, pp. 1427-1435, 2007.

[23] C. W. Oyster, *The human eye : structure and function*. Sunderland, MA: Sinauer Associates, 1999.

[24] P. C. Y. Chen and B. W. Zweifach, "Network reorganization - human bulbar conjunctiva in aging and disease," *Microcirculation, an update : proceedings of the Fourth World Congress for Microcirculation,* vol. 2, 1987.

[25] R. Derakhshani, A. Ross, and S. Crihalmeanu, "A New Biometric Modality Based on Conjunctival Vasculature," *Proc. of Artificial Neural Networks in Engineering,* 2006.

[26] M.-K. Hu, "Visual pattern recognition by moment invariants," *IRE Transactions on Information Theory,* vol. 8, pp. 179-187, 1962.

[27] R. Derakhshani and A. Ross, "A Texture-Based Neural Network Classifier for Biometric Identification using Ocular Surface Vasculature," in *Proc. of the Internationl Joint Conference on Neural Networks*, Orlando, FL, 2007, pp. 2982-2987.

[28] S. Crihalmeanu, A. Ross, and R. Derakhshani, "Enhancement and Registration Schemes for Matching Conjunctival Vasculature," in *Proceedings of the Third International Conference on Advances in Biometrics* Alghero, Italy: Springer-Verlag, 2009.

[29] C.-L. Lin and K.-C. Fan, "Biometric verification using thermal images of palm-dorsa vein patterns," *IEEE Transactions on Circuits and Systems for Video Technology,* vol. 14, pp. 199-213, 2004.

[30] J. Hashimoto, "Finger Vein Authentication Technology and Its Future," in *Symposium on VLSI Circuits*, 2006, pp. 5-8.

[31] X. Li, S. Guo, F. Gao, and Y. Li, "Vein Pattern Recognitions by Moment Invariants," in *The 1st International Conference on Bioinformatics and Biomedical Engineering*, 2007, pp. 612-615.

[32] W. Lingyu and G. Leedham, "Near- and Far- Infrared Imaging for Vein Pattern Biometrics," in *IEEE International Conference on Video and Signal Based Surveillance*, 2006.

[33] R. Sanchez-Reillo, B. Fernandez-Saavedra, J. Liu-Jimenez, and C. Sanchez-Avila, "Vascular Biometric Systems And Their Security Evaluation," in *41st Annual IEEE International Carnahan Conference on Security Technology*, 2007, pp. 44-51.

[34] Y. Ding, D. Zhuang, and K. Wang, "A study of hand vein recognition method," in *IEEE International Conference on Mechatronics and Automation*, 2005, pp. 2106-2110, vol. 4.

[35] Z. Yan, K. Wang, and N. Li, "An Algorithm for Extraction of Near Infrared Sublingual Veins," in *International Symposium on Computational Intelligence and Design*, 2008, pp. 60-63.

[36] G. Xu, Z. Zhang, and Y. Ma, "Automatic Iris Segmentation Based on Local Areas," in *18th International Conference on Pattern Recognition*, 2006, pp. 505-508.

[37] P. Li and X. Liu, "An incremental method for accurate iris segmentation," in *19th International Conference on Pattern Recognition*, 2008, pp. 1-4.

[38] C. Belcher and Y. Du, "Feature information based quality measure for iris recognition," in *IEEE International Conference on Systems, Man and Cybernetics*, 2007, pp. 3339-3345.

[39] W. W. Boles and B. Boashash, "A human identification technique using images of the iris and wavelet transform," *IEEE Transactions on Signal Processing*, vol. 46, pp. 1185-1188, 1998.

[40] Y. Du, "Review of Iris Recognition: Cameras, Systems, and Their Applications," *Sensor Review*, vol. 26, pp. 66-69, 2006.

[41] L. Ma, T. Tan, Y. Wang, and D. Zhang, "Personal identification based on iris texture analysis," *IEEE Transactions on Pattern Analysis and Machine Intelligence*, vol. 25, pp. 1519-1533, 2003.

[42] L. Ma, T. Tan, Y. Wang, and D. Zhang, "Efficient iris recognition by characterizing key local variations," *IEEE Transactions on Image Processing*, vol. 13, pp. 739-750, 2004.

[43] X. Liu, K. W. Bowyer, and P. J. Flynn, "Experiments with an improved iris segmentation algorithm," in *Fourth IEEE Workshop on Automatic Identification Advanced Technologies*, 2005, pp. 118-123.

[44] Z. Luo and T. Lin, "Detection of Non-iris Region in the Iris Recognition," in *International Symposium on Computer Science and Computational Technology*, 2008, pp. 45-48.

[45] J. R. Matey, R. Broussard, and L. Kennell, "Iris image segmentation and sub-optimal images," *Image and Vision Computing*, vol. (In Press), 2009.

[46] Q.-C. Tian, Q. Pan, Y.-M. Cheng, and Q.-X. Gao, "Fast algorithm and application of Hough transform in iris segmentation," in *Proceedings of the International Conference on Machine Learning and Cybernetics*, 2004, pp. 3977-3980, vol.7.

[47] T. Tan, Z. He, and Z. Sun, "Efficient and robust segmentation of noisy iris images for non-cooperative iris recognition," *Image and Vision Computing*, vol. (In Press), 2009.

[48] M. Vatsa, S. Richa, and P. Gupta, "Comparison of iris recognition algorithms," in *Proceedings of International Conference on Intelligent Sensing and Information Processing*, 2004, pp. 354-358.

[49] M. Vatsa, R. Singh, and A. Noore, "Improving Iris Recognition Performance Using Segmentation, Quality Enhancement, Match Score Fusion, and Indexing," *IEEE Transactions on Systems, Man, and Cybernetics, Part B: Cybernetics*, vol. 38, pp. 1021-1035, 2008.

[50] R. P. Wildes, "Iris recognition: an emerging biometric technology," *Proceedings of the IEEE*, vol. 85, pp. 1348-1363, 1997.

[51] Z. He, T. Tan, Z. Sun, and X. Qiu, "Toward Accurate and Fast Iris Segmentation for Iris Biometrics," *IEEE Transactions on Pattern Analysis and Machine Intelligence*, vol. 31, pp. 1670-1684, 2009.

[52] E. M. Arvacheh and H. R. Tizhoosh, "IRIS Segmentation: Detecting Pupil, Limbus and Eyelids," in *IEEE International Conference on Image Processing*, 2006, pp. 2453-2456.

[53] H. Proenca and L. A. Alexandre, "Iris segmentation methodology for non-cooperative recognition," *IEEE Proceedings - Vision, Image and Signal Processing*, vol. 153, pp. 199-205, 2006.

[54] H. Proenca, "Iris Recognition: On the Segmentation of Degraded Images Acquired in the Visible Wavelength," *IEEE Transactions on Pattern Analysis and Machine Intelligence*, 2009.

[55] H. Proenca and L. A. Alexandre, "Toward Noncooperative Iris Recognition: A Classification Approach Using Multiple Signatures," *IEEE Transactions on Pattern Analysis and Machine Intelligence,* vol. 29, pp. 607-612, 2007.

[56] M. Abdullah-Al-Wadud and C. Oksam, "Region-of-Interest Selection for Skin Detection Based Applications" in *International Conference on Convergence Information Technology,* 2007, pp. 1999-2004.

[57] M. Abdullah-Al-Wadud and O. Chae, "Skin Segmentation Using Color Distance Map and Water-Flow Property," in *Fourth International Conference on Information Assurance and Security,* 2008, pp. 83-88.

[58] T. H. Cormen, *Introduction to algorithms*, 3rd ed. Cambridge, MA: MIT Press, 2009.

[59] G. O. Williams, "Iris recognition technology," *IEEE Aerospace and Electronic Systems Magazine,* vol. 12, pp. 23-29, 1997.

[60] M. Li, T. Tieniu, W. Yunhong, and Z. Dexin, "Efficient iris recognition by characterizing key local variations," *Image Processing, IEEE Transactions on,* vol. 13, pp. 739-750, 2004.

[61] N. Van Huan and H. Kim, "A Novel Circle Detection Method for Iris Segmentation," in *Congress on Image and Signal Processing,* 2008, pp. 620-624.

[62] C. A. Corral and C. S. Lindquist, "On implementing Kasa's circle fit procedure," *IEEE Transactions on Instrumentation and Measurement,* vol. 47, pp. 789-795, 1998.

[63] R. C. Gonzalez, *Digital image processing*, 2nd ed. Upper Saddle River, NJ: Prentice Hall, 2002.

[64] K. Zuiderveld, "Contrast limited adaptive histogram equalization," in *Graphics gems IV*: Academic Press Professional, Inc., 1994, pp. 474-485.

[65] Q. Li, S. Sone, and K. Doi, "Selective enhancement filters for nodules, vessels, and airway walls in two- and three-dimensional CT scans," *Medical Physics,* vol. 30, pp. 2040-2051, 2003.

[66] J. Daugman, "Two-dimensional spectral analysis of cortical receptive field profiles," *Vision Research,* vol. 20, pp. 847-856, 1980.

[67] R. Hamming, "Error Detecting and Error Correcting Codes," *Bell System Technical Journal,* vol. 26, pp. 147-160, 1950.

[68] R. O. Duda, P. E. Hart, and D. G. Stork, *Pattern Classification*. New York: John Wiley & Sons, 2001.

[69] Y. Du, C.-I. Chang, H. Ren, C.-C. Chang, J. O. Jensen, and F. M. D'Amico, "New hyperspectral discrimination measure for spectral characterization," *Optical Engineering*, vol. 43, pp. 1777-1786, 2004.

[70] T. Cover and J. Thomas, *Elements of Information Theory*. Wiley-Interscience, 1991.

[71] M. A. Fischler and R. C. Bolles, "Random sample consensus: a paradigm for model fitting with applications to image analysis and automated cartography," *Commun. ACM*, vol. 24, pp. 381-395, 1981.

[72] L. Masek and P. Kovesi, "MATLAB Source Code for a Biometric Identification System Based on Iris Patterns," The School of Computer Science and Software Engineering, The University of Western Australia, 2003.